Novel ferrocene-appended β-ketoimines and related BF_2 derivatives with significant aggregation-induced emission and second-order nonlinear optical properties

Ezhumalai David,[a] Alessia Colombo,[b] Claudia Dragonetti,*[b] and Nallasamy Palanisami*[a]

[a] Dr. E. David, Prof. Dr. N. Palanisami
Centre for Functional Materials, Department of Chemistry,
School of Advanced Sciences,
Vellore Institute of Technology, Vellore 632014, Tamilnadu, India.
E-mail: palanisami.n@vit.ac.in; palanisami.n@gmail.com

[b] Dr. A. Colombo, Prof. Dr. C. Dragonetti
Dipartimento di Chimica dell'
Università degli Studi di Milano and UdR-INSTM,
Via C. Golgi 19, I-20133 Milano, Italy.
E-mail: claudia.dragonetti@unimi.it

Supporting information for this article is given via a link at the end of the document.

Abstract: A series of new β-ketoimines containing a ferrocene moiety and related BF_2 derivatives were synthesized and structurally characterized. The solvatochromism of the β-ketoimines was studied, putting in evidence a red shift by increasing the solvent polarity. This positive solvatochromism can be attributed to the more polarized excited state, with respect to the ground state, due to intramolecular charge transfer (ICT) transitions. β-ketoimines exhibit a weak emission, attributable to the excited state intramolecular proton transfer (ESIPT) phenomenon. This ESIPT effect is suppressed upon restriction of the keto-enamine tautomerism by addition of $BF_3{\cdot}OEt_2$ which affords the related BF_2 complexes, characterized by an enhancement of the fluorescence through the ICT effect. Both β-ketoimines and BF_2 complexes, examined in mixtures of CH_3CN/H_2O, exhibit a significant aggregation-induced emission (AIE) behavior, due to restriction of intramolecular rotation (RIR) in the aggregated state. The frontier molecular orbital levels, ground and excited state dipole moments (μ_g and μ_e), and the origin of electronic absorption spectra were studied by using time-dependent density functional theory (TD-DFT) calculations. The second-order nonlinear optical (NLO) properties were determined by the EFISH technique. The $\mu\beta_{1907}$ value of all β-ketoimines increases upon the formation of the related BF_2 complex, mainly due to an enhancement of the ground state dipole moment. Some of these novel compounds are excellent multifunctional candidates for NLO and luminescence applications.

Introduction

Nonlinear optics has been the subject of intensive research, because of its wide applications in the fields of photonics,[1-3] optoelectronics,[1-4] optical switching,[5-7] optical communications,[1-3] information storage,[1-3,8] and signal processing.[1-3,9] Although inorganic crystalline salts and conjugated organic molecules can be characterized by a high second-order nonlinear optical (NLO) response, inorganic salts suffer from uneasy structure manipulation ability whereas organic compounds suffer from poor thermal, mechanical and photochemical stability. The effort to address these disadvantages led to coordination compounds, where metal atoms and organic moieties were brought together to stabilize the structure and enhance the quadratic hyperpolarizability as well as thermal, mechanical and photochemical properties of the molecules.[10-12] To have a high second-order NLO response, a compound must be non-centrosymmetric, it should have charge-transfer transitions of low energy and there must be large variations of the dipole moment during electronic excitation.[1-3] Typically, molecules with electron-donor (D) and electron-acceptor (A) fragments coupled via a polarizable moiety can have a respectable NLO response.[1-3] In coordination compounds, the metal can act as the donor, the acceptor or even the polarizable bridge of the NLO-active system.[10-17] Among them, compounds having a ferrocene (Fc) moiety are of particular interest. Indeed, Fc is fascinating due to its donor properties, its easy chemical modification and its simple electrochemical reversible one-electron transfer behaviour.[18-20] Inspired by the important report of Green and Marder,[21] many investigations have exploited the ferrocenyl group as an electron donor to achieve significant NLO properties.[8, 22-31]

In the last few years, coordination compounds characterized by both luminescent and NLO properties are of growing interest as new molecular multifunctional materials.[32-37] In particular, materials with aggregation-induced emission (AIE) attributes, in which the light emission is induced by aggregates formation, have attracted much interest since the debut of the AIE concept discovered by Ben Zhong Tang et al. in 2001.[38, 39]

The unique AIE effect is usually originated from the mechanism of restricted intramolecular rotation (RIR). The rotor-containing AIE-luminogens undergo dynamic intramolecular rotations in dilute solutions, which lead to non-radiative pathways and fluorescence quenching, whereas, in the aggregated state, the rotations are restricted allowing an efficient radiative pathway for the excited state electrons back to ground state.[39] Recently, studies on AIE emissive derivatives with third-order nonlinear optical properties have gathered attention because of their wide applications in luminescent materials, chemosensors, organic photovoltaics, molecular probes, bioimaging, ion sensing and organic light emitting devices (OLEDs).[40] The development of molecules with both NLO and AIE properties is in its infancy and needs to be explored more deeply. It turned out that ferrocene compounds are of interest also in this field. Thus, some of us reported ferrocene-appended donor-π-acceptor Schiff bases characterized by both second-order nonlinear optical and AIE properties.[41]

In the search of novel molecular materials, combination of excited-state intramolecular proton transfer (ESIPT) with AIE is particularly fascinating because it represents an elegant way to overcome the limitations of many ESIPT dyes. In general, molecules can exhibit ESIPT fluorescence if their structures incorporate an intramolecular hydrogen bonding interaction between a hydrogen bond donor (–OH and NH_2) and a hydrogen bond acceptor (=N– and C=O). Common ESIPT fluorophores are analogues of 2-(2'-hydroxyphenyl) benzimidazole, 2-(2'-hydroxyphenyl)benzoxazole and 2-(2'-hydroxyphenyl)benzothiazole, but excited-state intramolecular proton transfer has also been observed for β-ketoimines.[42-44] ESIPT is a four-level photochemical process, with the electronic ground state of ESIPT fluorophores typically existing in an enol (E) form. Upon photoexcitation, the electronic charge of such molecules can be redistributed, resulting in greater acidity for the hydrogen bond donor group and increased basicity for the hydrogen bond acceptor within the E form. As a result, an enol to keto phototautomerization takes place, with the excited state enol form (E*) rapidly converting to its excited keto form (K*). After decaying radiatively back to its electronic ground state, a reverse proton transfer takes place to produce the original E form. ESIPT fluorophores can exhibit dual-emission spectra arising from the excited state enol (E*) and the excited state keto (K*) emissions.[42-43] In solution, intramolecular rotations can non-radiatively extinguish the excited states of ESIPT fluorophores whereas, in the aggregate form, the rigid environment favors the formation of hydrogen bonds and turns on the light emission.[44] These observations, the fascinating AIE behavior of boron ketoiminates[45] and the interesting NLO properties of a ferrocene-appended β-ketoimine,[11] prompted us to prepare and study novel ferrocene-appended β-ketoimines and related BF_2 derivatives (see compounds in Scheme 1), for both aggregation-induced emission and second-order nonlinear optical behavior. Their structures have been determined by single crystal X-ray diffraction (XRD), and their electronic absorption spectra and electrochemical properties have been experimentally investigated. The optical properties have also been computed by employing density functional theory (DFT/TD-DFT) calculations, revealing a good correlation between theoretical and experimental data. The second-order NLO responses were measured by means of the electric-field induced second harmonic generation (EFISH) technique.

Results and Discussion

Synthesis and characterization

β-Ketoimines are readily prepared by reaction of 1-(4,4,4-trifluoromethyl-1,3-dione) ferrocene, synthesized as previously reported,[46] with the suitable amine (Scheme 1). Further reaction with $BF_3.Et_2O$ in dichloromethane at room temperature leads to the related purple BF_2 complexes (**BF1-BF4**), which can be purified by column chromatography (52-56% yields), like previously reported in the case of β-diketonate derivatives.[47]

The ^{1}H NMR spectra of β-ketoimines (**L1-L4)** and related BF_2 complexes **(BF1-BF4)** display the ferrocenyl fragment which shows three signals: two doublets in the range δ 4.14-5.00 ppm which are assigned to protons of the substituted cyclopentadienyl ring, and one singlet at 4.08-4.33 ppm, due to the unsubstituted cyclopentadienyl ring protons for both β-ketoimines and BF_2 complexes. Most characteristic is the appearance of a singlet signal at δ 5.85–6.79 ppm for the methine (COCHCN) that evidences the presence of a keto-enamine tautomer in the structure. The aromatic zone in the ^{1}H NMR spectra (NMR spectra are shown in Figures S2-S29) show two doublets (**L2**-**L4** and **BF2**-**BF4**) and triplets (**L1**-**BF1**) in the range δ 6.75–8.17 ppm, as expected for the phenyl moiety. The β-ketoimines are obtained as their enaminone tautomeric forms, as deduced from their deshielded amino proton signal at δ_H 11.91, 11.64, 11.99 and 12.08 ppm, for **L1, L2, L3, and L4,** respectively. This proton is associated with the hydrogen bonding between N-H and the carbonyl oxygen atom through an intramolecular hydrogen-bonding interaction.[48-49] The ^{13}C NMR spectrum of β-ketoimines (**L1-L4)** in $CDCl_3$ confirms the existence of the keto-enamine tautomeric form. The methine carbon resonates at 92.4-97.7 ppm for the keto-enamine form. In addition, C_{ipso} carbon of substituted cyclopentadienyl ring displays in the range at 79.3-81.7 ppm for the β-ketoimines and BF_2 complexes. Further the fluorine attached carbon in CF_3 group is confirmed by quartet [$^1J_{C\text{-}F}$ (270-290 Hz) around 115-120 ppm. Whereas, another quartet [$^2JC\text{-}F$ (30-36 Hz)] belongs to iminic carbon in the range δ 143-146 ppm. At the same time, (C=O) experiences a downfield shift from 194.96 to 173.65 ppm after the formation of BF_2 complexes. The β-ketoimines and related BF_2 complexes were further characterized by ^{11}B and ^{19}F NMR spectroscopy. The observed chemical shift in the ^{11}B NMR spectra of boron difluoride complexes is at ca –32 ppm whereas the ^{19}F NMR signal is around −137 ppm, in agreement with similar complexes.[50]

The HR-mass spectra of β-ketoimines and complexes

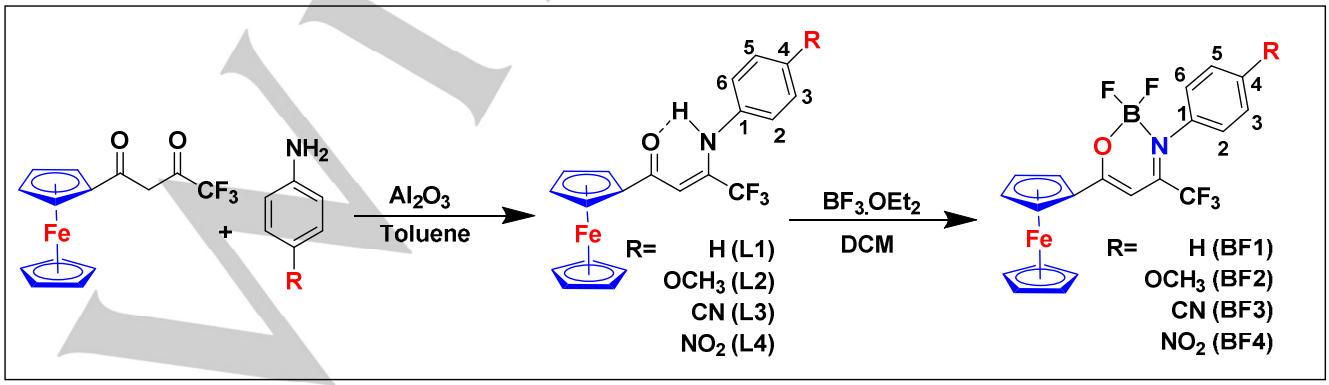

show a peak with the expected isotopic pattern at m/z =

399.0554 (for **L1**), 429. 0662 (for **L2**), 424.0506 (for **L3**), 444.0407 (for **L4**) and

Scheme 1. Synthesis of β-ketoimines **L1-L4** and related BF_2 complexes **BF1-BF4**.

BF_2 complexes, 447.0541 (for **BF1**), 477.0648 (for **BF2**), 472.0493 (for **BF3**), and 492.0392 (for **BF4**), in agreement with calculated data (Figures S30-S37).

The FT-IR spectra (Figure S38 and S39) exhibit a weak band at around 3250 cm^{-1} which is attributed to the stretching vibration of the hydrogen-bonded enamine N–H group.[51] Moreover, a characteristic band at 750 cm^{-1} is attributed to the aromatic δ(C–H) mode associated with the para substitution. The imine (C=N) and (N–H···O) vibrations at 1642 cm^{-1} and 1517 cm^{-1} of free β-ketoimines are shifted to 1629 cm^{-1} and 1571 cm^{-1} upon complexation with boron. As expected, the N–H absorption bands have disappeared in the spectra of BF_2 complexes, indicating coordination through nitrogen atoms by deprotonation. The C–F stretching vibration was observed in the range 1100-1200 cm^{-1} for all the compounds. Further, β-ketoimine L4 and the corresponding boron complex show strong strecthing vibration in at range of 1500 and 1300 cm^{-1}, corresponding to asymmetric and symmetric stretching vibration of N–O group, respectively. Besides, the presence of B–O and B–N vibration peaks at 1178 cm^{-1} and 1028 cm^{-1} are in agreement with the formation of boron complexes.

Crystallography structure of L1-L3 and BF1

Crystals of β-ketoimines **L1-L3** and complex **BF1**, suitable for single-crystal X-ray diffraction studies, were obtained by slow evaporation of the solvent from their saturated solution in ethyl acetate/hexane and the structural refinements details were summarized in Table S1. The molecular structures are shown in Figure 1, and selected bond lengths and angles are listed in Table S2. The measured cyclopentadienyl ring centroid-iron distances, averaging 1.646 and 1.658 Å in **L1** and 1.632 and 1.652 Å in (**BF1**), for the unsubstituted and substituted ring, respectively, are in agreement with a Fe(II) oxidation state in the metallocene units. The crystal structures of β-ketoimines **L1-L3** and of complex **BF1** show that the angle of the cyclopentadienyl rings in ferrocene moieties are eclipsed, with twist angles of 0.11° for **L1**, 2.31° for **L2**, 0.43° for **L3** and 0.25° for **BF1**. The overlap pictograms of the aromatic rings and other inter and intramolecular interactions (hydrogen bonding and π···π interactions) are shown in Figure 2 and Figure S40. The phenyl ring is deviated from planarity, with respect to the monosubstituted cyclopentadienyl ring of the ferrocene unit, by 24.26° (**L1**), 24.83° (**L2**), 22.43° (**L3**) and 33.46° (**BF1**). The cyclopentadienyl ring of ferrocenyl β-ketoimine has an interplanar angle of 63.80° for **L1**, 84.10° for **L2**, 86.55° for **L3** and 24.89° for **BF1**.

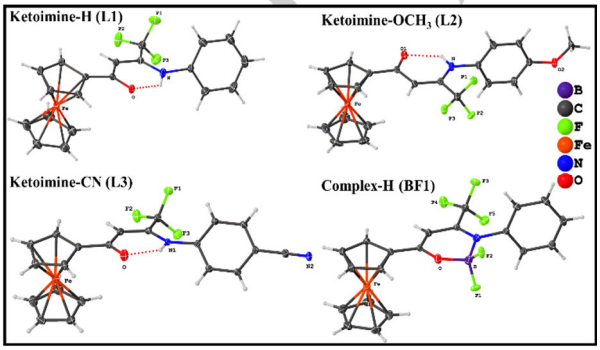

Figure 1. Molecular structure of β-ketoimines **L1-L3** and complex **BF1** (with 50% probability ellipsoids).

The β-ketoimines analyzed in this work crystallized in the centrosymmetric $P2_1/c$ and $P\bar{1}$ space groups that belong to the monoclinic (**L1, L3**) and triclinic(**L2**) crystal system. In the cyclopentadienyl ring centroid-Fe-centroid angles are 178.43° (**L1**), 177.81°(**L2**), 178.31° (**L3**) and 175.39° (**BF1**). The molecular structure of **L1-L3** is in agreement with a keto-enamine tautomeric isomer and an intramolecular O…H–N hydrogen bond that closes the planar pseudo six-membered [O=C–C=C–N] chelate ring through the resonant ···O=C–C=C–NH··· fragment with alternating double and single bonds between the vicinal sp^2-hybridized atoms. In addition, in the ketoimine framework [O=C–C=C–N], the angles [C–C=C] are in the range of 120.1° to 123.0°, [O=C–C] are between 120.8° to122.0°, whereas [C=C–N] values are between 122.0° to 123.6°. These values are very close to ideal planar of 120° and it can be further considered as sp^2-hybridized form of ketoimine framework.[11]

The boron difluoride complex **BF1** crystallizes in the monoclinic system and centrosymmetric space groups $P2_1/c$, with a single molecule in the asymmetric unit. Angles of F–B–F 111.4(3), B–N (ϕ = 120.02), B–O (ϕ = 124.35), B–F (ϕ = 111.39) and the average bond length is 1.557(4) Å, 1.473(4) Å, 1.354(5)Å, respectively. The chelated ring adopted a puckered conformation, owing to the nature of the nitrogen and oxygen atoms, with torsional angles in the range of ϕ = 120.6-128.3. Also, the dihedral angles (ω) between the mean planes defined by the N-bonded arene and the boron heterocycle ring, along with crystal packing structures, are shown in Figures S41 and S42. The arene π–π stacking was evident, with closest π–π interplanar distance of 3.856 Å. Angles CH···π and intermolecular CH···F were 151.36 and 158.55, respectively

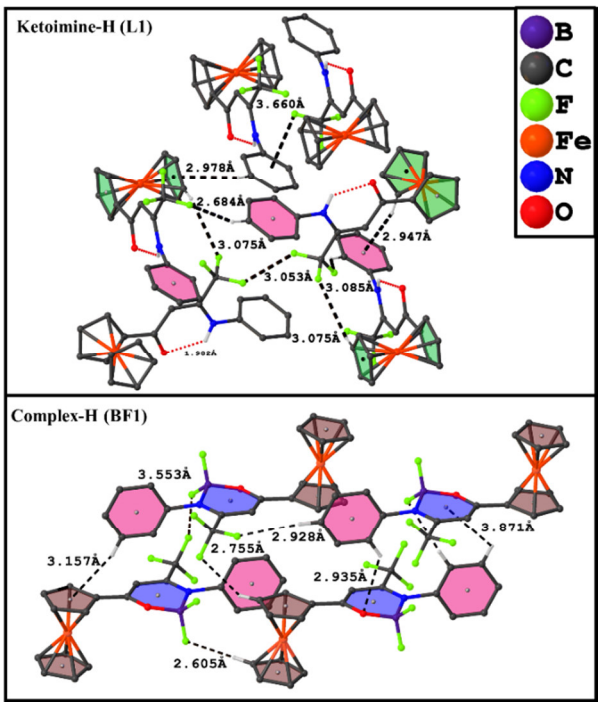

(Figures 2 and S40). Besides, CH···F distances in the order of 2.684 Å, for **L1**, and 2.755 Å, for **BF1**, were observed in the lattices of these compounds. These interactions could affect photophysical relevant electronic states of all the chromophores, as confirmed by DFT optimized structures (see **L1-L4** and **BF1-BF4** in Figure S43).

Figure 2. Intermolecular interactions of (C–H···π, C–H···F, C–F···F, and C–F··· π) ferrocenyl ketoimine (**L1**) and -BF_2 complex (**BF1**) (hydrogen atoms omitted for clarity)

Electrochemical Studies

The electrochemical features of β-ketoimines (**L1**-**L4**) and BF_2 complexes (**BF1**-**BF4**) were investigated by cyclic voltammetry in an acetonitrile solution containing $[N(C_4H_9\text{-}n)_4]ClO_4$ as supporting electrolyte. All measurements were carried out in 10^{-5} M solutions at room temperature in the potential range of 0 to 1.0 V with a scan rate 50 mV s^{-1}. The electrochemical data for these compounds are shown in Table S3. It can be seen that the β-ketoimines and BF_2 complexes exhibit one-electron redox couple, the redox potentials being shifted to a positive potential in comparison with unsubstituted ferrocene. Cyclic voltammograms (CV) of solution containing β-ketoimines (**L1**-**L4**) and complexes (**BF1**-**BF4**) show a chemically quasi-reversible process with current ratio i_{pa}/i_{pc} not close to unit; half-wave potential value [$E_{1/2} = (E_{pa} + E_{pc})/2$] of all compounds are more positive, as shown in Figures 3 and S44. An anodic reversible wave at $E_{1/2}$ = 793-816 mV, attributed to the oxidation of the ferrocenyl group, was observed. This E value is 111 mV positively shifted with respect to that of ferrocene ($E_{1/2}$ = 492 mV), thus illustrating the electron-withdrawing properties of the delocalized organic substituent in a para position of the aryl ring. Therefore, it appears that the potential of the oxidation process, which is centered on the ferrocenyl moiety, is only slightly affected by the electronic effects induced by the substituent of β-ketoimines and BF_2 complexes. Electrochemical potentials for second-order NLO chromophores provide information about the highest occupied molecular orbital (HOMO) energy level. From the oxidation potential (E_{ox}), HOMO was calculated using the relationship $E_{HOMO} = -(E_{ox} + 4.4)$.[52]

Photophysical properties

The absorption spectra of the ferrocenyl substituted β-ketoimines (**L1-L4**) and -BF_2 complexes **(BF1-BF4)**, recorded in CH_3CN at room temperature, are shown in Figures S45 and S46. Related data are listed in Table 1. The ferrocenyl β-ketoimines and BF_2 complexes show the higher energy (HE) bands at 257-276 nm which may be attributed to the π−π* transition. 322-344 nm n−π* transition from the imine to the substituent phenyl moiety.[53] Whereas weak low energy band at 449-451 nm is attributed to metal-to-ligand charge transfer (MLCT) and d–d transitions arising from the ferrocene moiety.[54]

Figure 3. Cyclic voltammograms of BF_2 complexes (**BF1-BF4**) oxidation and reduction process were measured in CH_3CN (glassy carbon working electrode, scan rate = 50 mVs^{-1}).

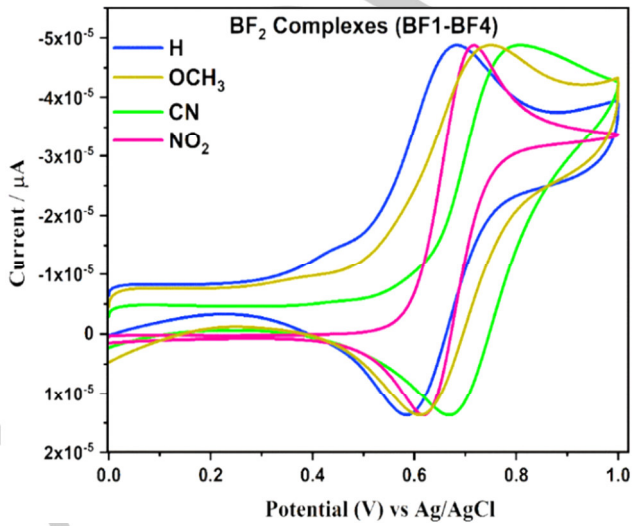

Solvatochromism

Solvatochromic studies have been carried out on β-ketoimines **L1-L4**, by using solvents with different polarities. The wavelength maxima (λ_{max}) changes of β-ketoimines with solvent polarity were compared with the α (hydrogen bond donor), β (hydrogen bond acceptor), and π* (polarizability) solvent parameters, as determined by Kamlet and Taft (Table S4).[55] An increase of the solvent polarity from THF to DMSO leads to a positive solvatochromism of the absorption spectra of β-ketoimines with red-shift of the λ_{max}= 51 (**L1**), 61 (**L2**), 52 (**L3**) and 37 (**L4**) nm values (Figures S47-S50), highlighting that polar solvents can lead to a better stabilization of a polarized excited state, arising from an extended intramolecular charge transfer (ICT) from the ferrocenyl donor to the acceptor moieties.[56] The red shift of λ_{max} values on increasing the solvent polarity reveals an increase in the dipole moment upon excitation, in agreement with the results of TD-DFT calculations (Table 2), which predict that the excited states should be more polar than the ground states for these β-ketoimines.[57]

Figure 4. (a) UV-Vis and (b) fluorescence spectra of **L1** (1 x 10^{-5}) upon addition of $BF_3.OEt_2$; red and green curves for 0 and 150/270 μm $BF_3.OEt_2$, respectively.

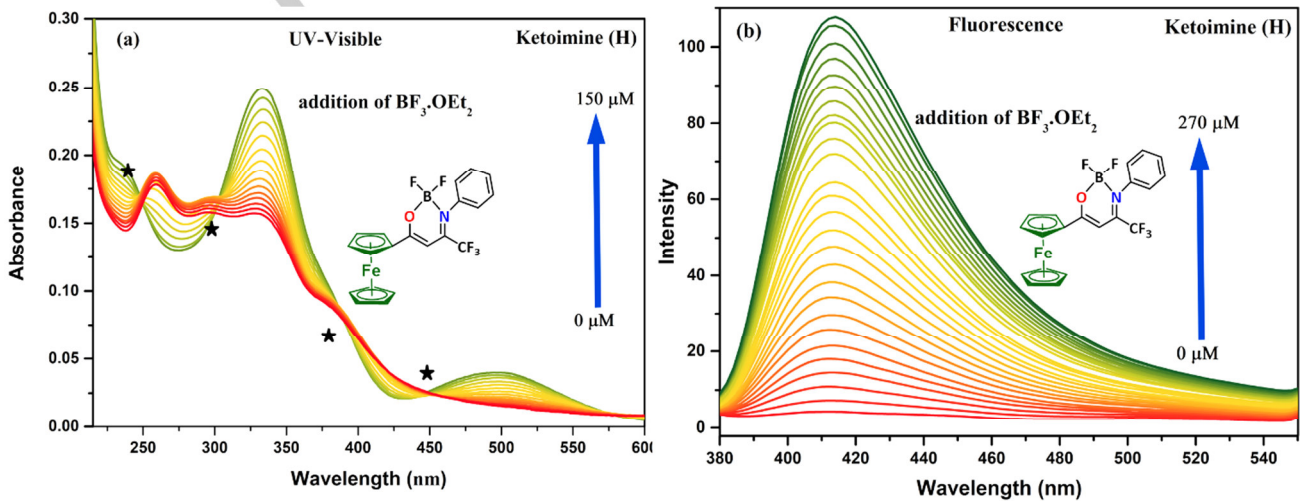

Formation of BF_2 complex

The ESIPT process generally involves the transfer of a hydroxyl (or amino) proton to a carbonyl oxygen (or imine nitrogen) less than 2Å away through a pre-existing six- or five- membered ring hydrogen bonding configuration.[44] The chromophores often exhibit weak emission due to the excited state intramolecular proton transfer (ESIPT) phenomenon, where the ESIPT effect can be suppressed under the restriction of the keto–enol tautomerism with concomitant increase of the fluorescence intensity through intramolecular charge transfer (ICT) effect.[58]

The UV−Vis spectra of representative β-ketoimine **L1** upon addition of $BF_3.OEt_2$ (0-150 mM) is illustrated in Figure. 4a. The UV-Vis spectrum before the addition of boron trifluoride exhibits an absorption band at 259 nm with a shoulder at 330 nm, ascribed to the ketoimine moiety. Increase in the concentration of $BF_3.OEt_2$ leads to the appearance of a new bathochromic shift at 274 and 334 nm corresponding to the BF_2 complex. This hyperchromic and hypochromic effect of the absorption band formation of isobestic points were attributed to the intermolecular proton transfer between the O atom of the hydroxyl group and the N atom of imine moiety, important sites to form an intermolecular hydrogen bond with the BF_2 moiety, which might affect greatly the excited-state intramolecular proton transfer.[60]

The fluorescence behavior of β-ketoimine **L1** is probably due to the lone pair of electrons on the nitrogen atom in conjugation with the phenyl group. Upon addition of $BF_3.OEt_2$. (0-270 mM), an increase with a slight red shift of the fluorescence emission band at 413 nm is observed along with a color change from yellow to violet (Figure. 4b). The emission quantum yields of **L1** and related BF_2 complex were determined in CH_3CN, taking quinine sulfate in 0.1 M H_2SO_4 as reference. As expected for the restriction of the keto-enamine tautomerism and for an increase of the rigidity,[59] the quantum yields of ketoimines are greatly enhanced (ten-fold enhancement) upon formation of the boron difluoride complexes (see Table 1). The formation of the BF_2 complex, in CH_3CN solution, was studied using the Benesi-Hildebrand plot of the fluorescence intensity as a function of the $BF_3.OEt_2$ concentration (Figure 5). The Benesi-Hildebrand equation in terms of *Ka* (association constant) for complexation of ketoimine to BF_2 is 1.01 x 10^{-2} (**L1**) M.

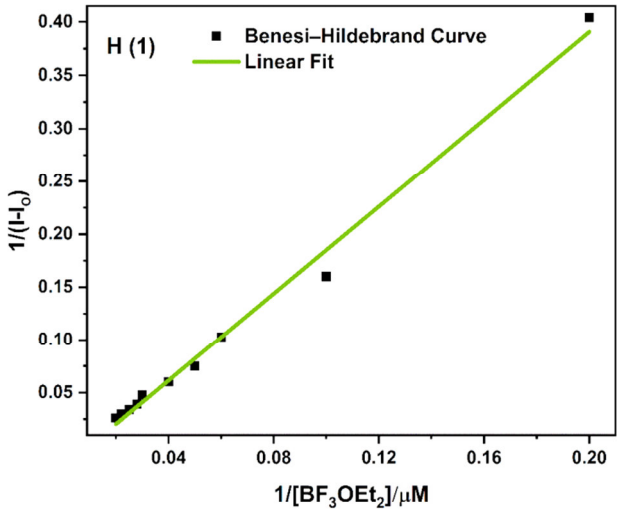

Figure 5. Benesi-Hildebrand plot for complexation of ketoimine **L1** to **BF2**

Aggregation-induced emission (AIE)

Our novel β-ketoimines and BF_2 complexes, dissolved in CH_3CN, are characterized by a relatively weak fluorescence (Figures S51 and S52). Their potential AIE properties were investigated in water/CH_3CN mixtures. The emission spectra of β-ketoimines and complexes were recorded in the presence of different water fractions, ~f_w= 0–90%, maintaining the overall concentration of the solution at 10^{-4} M. intensity of β-ketoimines and complexes increases drastically upon increasing the water fraction up 90%. On increasing the water fraction in the solution, a better restriction of movement of the ketoimine group may be the reason for blocking non-radiative pathways and subsequently opening up several new radiative pathways.[61] Thus, the restriction of intramolecular rotation (RIR) is one of the plausible mechanisms of AIE activity.[39,62]

Table 1. UV-Visible absorption, fluorescence, quantum yield and lifetime data for ketoimines and complexes.

Entry	λ max, abs (nm)[a]	λ max, fl (nm)[b]	Stoke's Shift (cm^{-1})[c]	Quantum yield (CH_3CN) (Φ_{fl})[d]	AIE Quantum yield (CH_3CN/H_2O)[e] (Φ_{fl})[d]	τ_ϕ (ns)[f]
L1	276, 326, 484	413	5548	0.001	0.022	3.6
L2	269, 324, 517	449	6798	0.001	0.024	5.7
L3	271, 327, 514	415	5754	0.001	0.023	5.2
L4	268, 322, 515	414	5786	0.001	0.022	3.7
BF1	272, 336, 486	449	2854	0.013	0.202	4.4
BF2	267, 344, 514	462	3930	0.014	0.330	9.1
BF3	265, 335, 519	435	3749	0.014	0.341	5.6
BF4	257, 334, 533	438	4566	0.006	0.288	4.5

[a]The UV-Visible and FL Experiments were performed in CH_3CN solvents.
[b]Excitation at 375 nm.
[c]Δss = UV-Visible and FL.
[d]Quantum yields were reported relative to quinine sulphate (Φ_{fl} = 0.54 in 0.1M H_2SO_4). [e]CH_3CN/H_2O=1/9 v/v.
[f]Fluorescence lifetime was measured by exciting the samples at 375 nm using time-correlated single-photon-counting technique using 150 ns nanoleds.

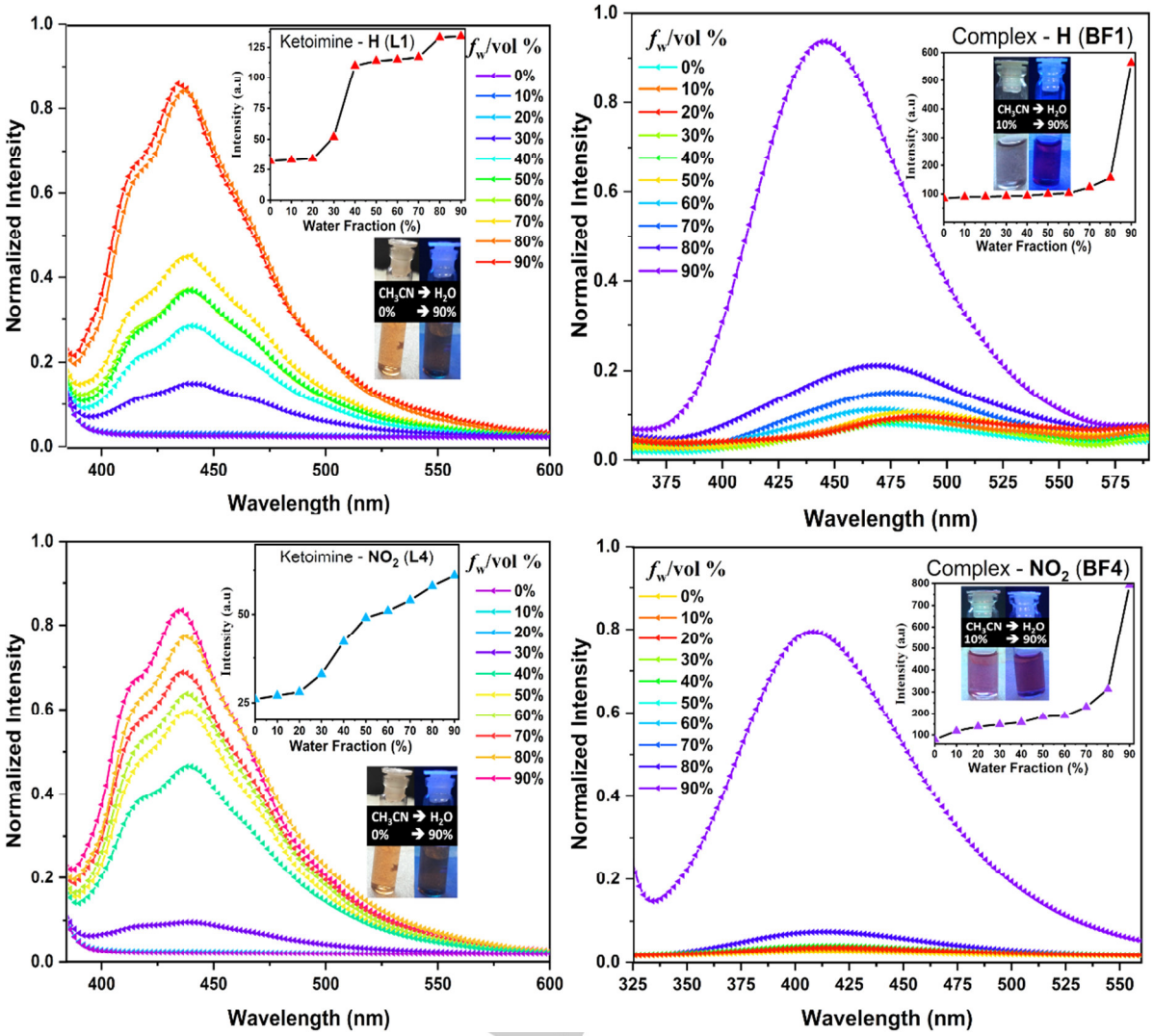

Figure 6. The fluorescence spectra of ketoimines (**L1**, **L4**) and BF_2 complexes (**BF1**, **BF4**) in different water fractions (f_w) at a concentration of $1x10^{-4}$ M.

Furthermore, π–π stacking of ketoimines and complexes, with increasing aggregation, may lead to enhancement of the emission intensity (Figures 6 and S53). Remarkably, a large increase (enhancement factor of 22-24) of the quantum yield of β-ketoimines (10^{-4} M) is observed by using CH_3CN/H_2O (1/9 v/v) instead of pure CH_3CN as solvent, due to the formation of the aggregates (Table 1). Similarly, the quantum yield of the BF_2 complexes increases by addition of water, the highest enhancement (factor of 48) being observed for **BF4** (Table 1). This AIE effect is much larger than that previously observed in the case of ferrocenyl Schiff bases (enhancement of quantum yields by a factor of 4-9 upon addition of a suitable amount of water).[41]

These results prompted us to study more deeply the aggregation phenomenon of β-ketoimines and related BF_2 complexes in the presence of CH_3CN/H_2O mixtures. High-resolution transmission electron microscopy (HR-TEM) was applied to study **L4** and related **BF4,** obtained by drop-casting their solution, either in pure CH_3CN or in a CH_3CN/H_2O (1/9 v/v) mixture, on a copper grid. It turned out that the HR-TEM images obtained from the CH_3CN/H_2O mixture show the presence of spherical aggregates with a size of 4-6 nm. These black spherical nanosized "AIE dots" are due to the high electron density of **L4** and **BF4**. They are not present when the chromophores are dissolved in pure CH_3CN (Figure 7). Therefore, the aggregation-enhanced PL emission response observed on going from the non-aggregate (0% water) to the aggregate state (90% water) is confirmed by morphology changes in HR-TEM images, which show that there are nano-sized AIE dots in the presence of water only. With this AIE phenomenon, since interactions with water and acetonitrile molecules dictate non-radiative decays, aggregation must deactivate non-radiative emission.[63] For the non-aggregated chromophores uniformly dispersed in the solution, a significant amount of excitation is non-radiatively dissipated in the surrounding solvent. When aggregated, the interactions between the AIE dots at the center of the aggregates and solvent molecules are reduced and, consequently, the PL intensity increases significantly.

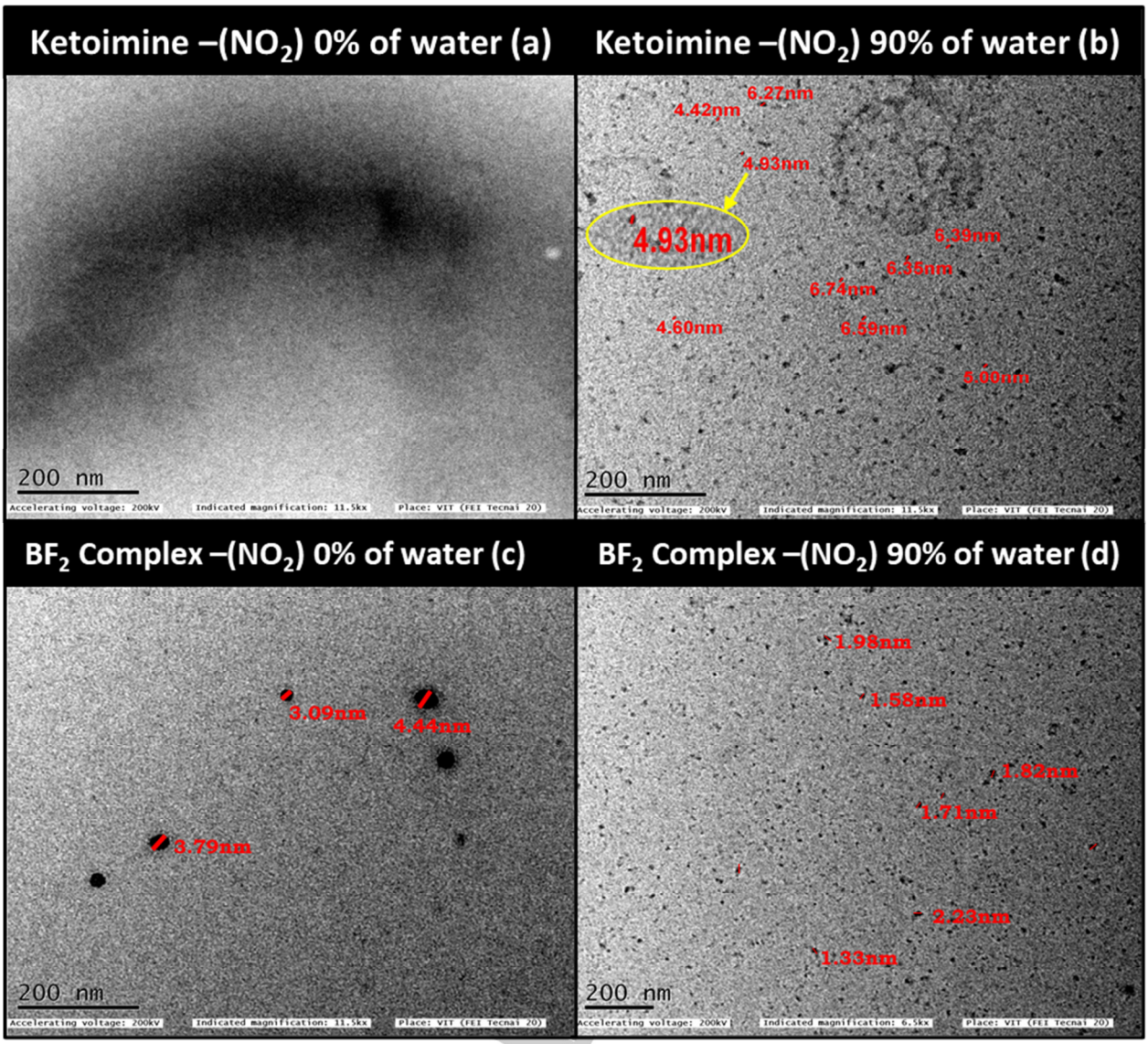

Figure 7. The HR–TEM images of **L4** and **BF4** indicate the size of the AIE dots to be around 4-6 nm.

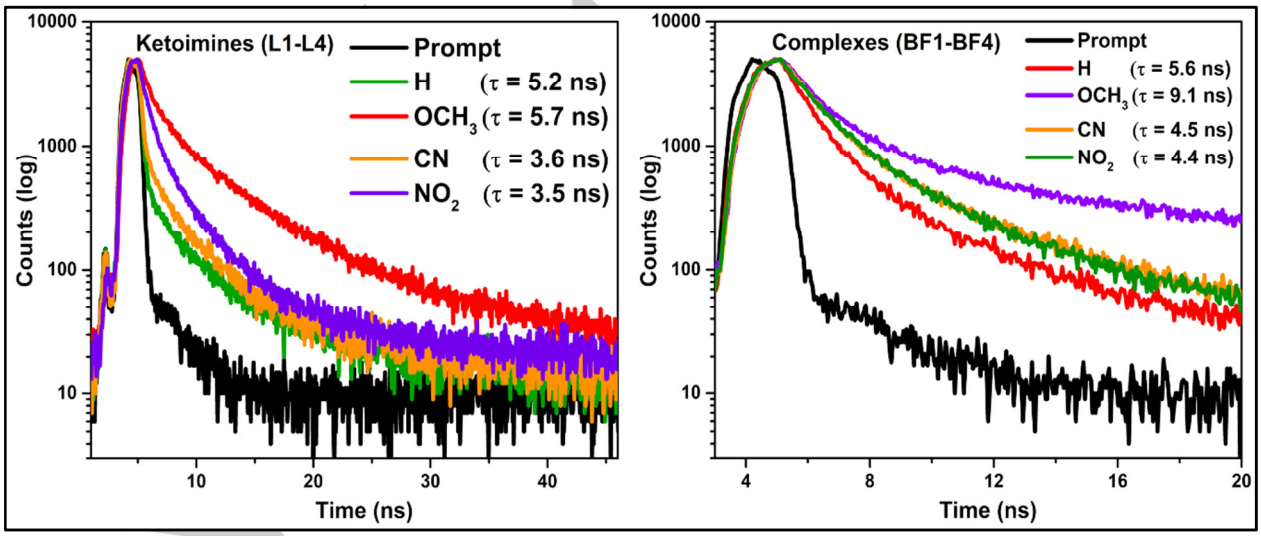

Figure 8. Time-resolved luminescence spectra of β-ketoimines and complexes (**L1-L4** and **BF1-BF4**) in CH_3CN/Water mixture (10/90).

Time-resolved fluorescence

Time dependent fluorescence decay measurements were carried out by the time-correlated single-photon counting (TCSPC) technique at 375 nm, as shown in Figure 8. The electron transfer time was calculated by fitting a biexponential function[64] to the fluorescence decay using eqs 1 and 2.

$$f(t) = \alpha_1 \exp(-t/\tau_1) + \alpha_2 \exp(-t/\tau_2) \qquad (1)$$

$$(\tau) = (\alpha_1\tau_1 + \alpha_2\tau_2)/+(\alpha_1/\alpha_2) \qquad (2)$$

where τ_1 and τ_2 are the fluorescence lifetime of the fast decay component and slow decay component, respectively, and α_1 and α_2 are the corresponding amplitudes.[65,66] The fluorescence decay time constants are provided in Table S5. The emission decay profiles of β-ketoimines and related BF_2 complexes were measured to monitor the local environment for AIE luminogens in aggregate states. In particular, a ferrocene-based molecule has increased electron donation due to $Fe^{2+} \leftrightharpoons Fe^{3+}$, which could result in the appearance of an intermolecular charge transfer (ICT) state and contribute to the weak emission. The excited state non-radiative relaxation of electron from non-aggregated to aggregated states is also an important process in the whole excited state dynamic events of β-ketoimines and BF_2 complexes. The lifetimes of β-ketoimines and complexes were all fit to biexponential decays, indicating emission from multiple species. However, in the case of water/CH_3CN mixtures, β-ketoimines and BF_2 complexes showed biexponential decay with the species having higher lifetimes 5.7 ns for **L2**, 9.1 ns for **BF2** (Table 1). In **L2** and **BF2**, the methoxy group is electron-donor and it can delocalize energy along the linkers, leading to the highest lifetime decay through mesomeric effect (+M).[67] In the case of β-ketoimines, the keto-enamine tautomerism units provide an ideal pathway for the fast decay of the exciton during the photoexcitation process. In the case of related BF_2 complexes, there is a slower lifetime decay attributed to the decrease in non-radiative decay modes, such as vibrations and rotations, due to constraints imposed by coordination to BF_2 which prevents keto-enamine tautomerization.

DFT and TD-DFT calculations

The effect of the nature of the solvent on the spectroscopic properties of β-ketoimines and BF_2 complexes can be explained by studying the difference between HOMO and LUMO. Also, frontier molecular orbitals (FMO) are very useful to get information about the excitation properties of molecules. The FMO orbital levels, electronic spectra, excited energies, oscillator strengths, and associated orbital transitions of β-ketoimines and complexes were determined by time-dependent density functional theory (TD-DFT) calculations, performed on the ground-state (singlet) geometry.

The calculated FMO energy levels, along with the HOMO–LUMO gaps, of β-ketoimines and BF_2 complexes are depicted in Figures 9 and 10. The intramolecular charge transfer (ICT) character of a D−π−A system depends on the spatial overlap between HOMO and LUMO. The HOMO and LUMO distributions of β-ketoimines (**L1**-**L4**) and its boron trifluoride complexes (**BF1**-**BF4**) exhibit different energy levels due to introduction of a -BF_2 unit in the β-ketoimines bring the lower energy HOMO and LUMO distributions. Thus, the LUMO of β-ketoimines is mainly localized on keto-enamine and phenyl moieties whereas, for the BF_2 complexes, the LUMO is well distributed on the difluoro and phenyl moieties, because of the strong electron-withdrawing ability of the BF_2 group. For this reason, the LUMO level of the BF_2 complexes is much deeper than that of the corresponding β-ketoimines. The HOMO energy determined experimentally from cyclic voltammetry is in agreement with the theoretical values (Table 2)[68,69] β-Ketoimines have higher HOMO-LUMO gaps than the corresponding BF_2 complexes, as expected for lower ICT properties. The highest gap is for **L2** bearing the methoxy group (3.74 eV, Figures. 9 and 10). BF_2 complexes have lower HOMO-LUMO gaps, due to the electron-withdrawing ability of the BF_2 moiety, the lowest gap being observed for **BF4** bearing the NO_2 group.

As can be seen in Figure S54 and Tables S6-S7, the HOMO is localized on the ferrocene moiety whereas the LUMO and LUMO+1 is centered on the imine and -BF_2 fragments. Therefore, these transitions have a significant CT character for all β-ketoimines and complexes. The relatively strong higher energy (HE) bands $S_0 \rightarrow S_1$ transitions (Table S8) are mainly attributed to the transitions from HOMO to LUMO, highlighting the intramolecular charge transfer character of the HE band.[70] Besides, the ground (μ_g) and excited (μ_e) electronic dipole moments were calculated for all β-ketoimines and complexes (Table 2). The highest values are for **BF4** with the NO_2 substituent (9.928 and 10.373 Debye, for μ_g and μ_e, respectively; Table 2).

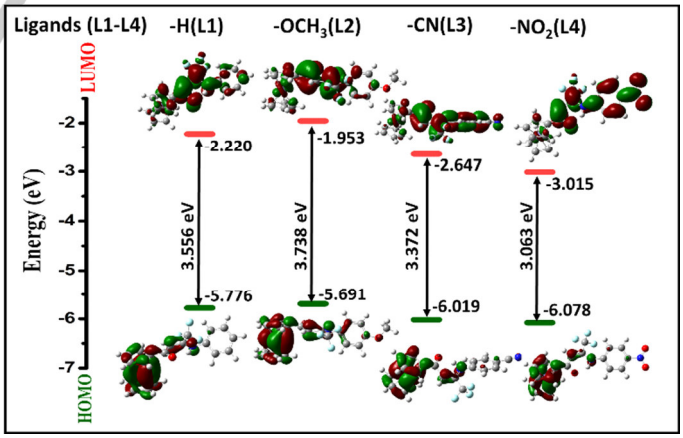

Figure 9. Molecular orbitals and energy levels of β-ketoimines **L1-L4** calculated at B3LYP/6-31+G** basis set.

Table 2. Comparison of experimental (CV/UV-Vis) and calculated (TD-DFT) HOMO-LUMO energy data and dipole moments; second-order NLO properties

	Experimental data					Theoretical data calculated (DFT/TD-DFT)					
Entry	**λ(nm)**[a]	E_{HOMO}[b] **(eV)**	$E_g^{optical}$[c] **(eV)**	$\mu\beta_{1.907}$[d] **(x10^{-48}esu)**	$\beta_{1.907}$[d] **(x10^{-30}esu)**	E_{HOMO}[e] **(eV)**	E_{LUMO}[e] **(eV)**	B.G[e] **(eV)**	$\mu_{g[D]}$[f]	$\mu_{e[D]}$[f]	$\Delta\mu_{eg[D]}$[f] **(x10^{-18}esu)**
L1	403	-5.09	3.076	234	210	-5.776	-2.220	3.557	1.116	1.448	0.332
L2	383	-5.18	3.237	470	460	-5.691	-1.953	3.739	1.021	1.048	0.027
L3	384	-5.21	3.229	355	50	-6.019	-2.647	3.371	7.055	7.683	0.628
L4	383	-6.11	3.229	625	73	-6.078	-3.015	3.064	8.574	10.351	1.207
BF1	396	-6.24	3.131	345	82	-6.063	-2.754	3.309	4.217	5.103	0.886
BF2	384	-6.26	3.229	540	79	-6.177	-2.939	3.238	6.830	7.632	0.802
BF3	356	-6.23	3.483	475	48	-6.283	-3.087	3.195	9.830	10.334	0.504
BF4	418	-6.27	2.966	810	82	-6.008	-3.262	2.743	9.928	10.373	0.443

[a]Calculated as λ^{onset} values are from absorption graphs in CH_3Cl solvent
[b]Calculated as HOMO level obtained from CV using Eqs
[b]$E^{optical}$ onset values obtained from oxidation peak in a cyclic voltammogram.
$E_{HOMO} = -e[E_{ox}^{onset} + 4.4]$
[c]Calculated as optical band gap calculated from absorption onset/edge using the equation.
$[E_g^{optical}] = 1240/\lambda_{onset}$
[d]In anhydrous $CHCl_3$, estimated uncertainty in EFISH measurement is 10%, [d]β_λ was calculated using the computed μ_g value.
[e]Theoretically calculated HOMO, LUMO and band gap values from DFT calculations
[f]Theoretically calculated dipole moment difference between the excited and ground state and from TD-DFT.

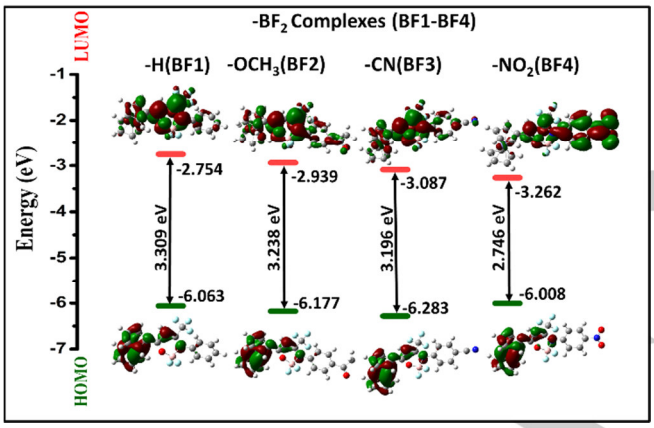

Figure 10. Molecular orbitals and energy levels of BF_2 complexes **BF1-BF4** calculated at B3LYP/6-31+G** basis set.

Second-order nonlinear optical properties

The second-order nonlinear optical properties of β-ketoimines and BF_2 complexes were determined by means of the EFISH technique[71-73] which can provide direct information on the intrinsic molecular NLO properties through eq. 3

$$\gamma_{EFISH} = (\mu\beta_\lambda/5kT) + \gamma(-2\omega;\omega,\omega,0) \qquad (3)$$

where $\mu\beta_l/5kT$ is the dipolar orientational contribution, λ is the fundamental wavelength of the incident photon in the EFISH experiment; $\gamma(-2\omega;\omega, \omega, 0)$, a third-order term at frequency ω of the incident light, is the cubic electronic contribution to γ_{EFISH}, which is usually negligible for dipolar complexes; β_λ is the projection along the dipole moment axis of the vectorial component β_{VEC} of the tensor of the quadratic hyperpolarizability whereas μ is the ground state dipole moment.[16] To avoid overestimation of the β value due to resonance enhancements, it is essential to choose an incident wavelength whose second harmonic is remote from any absorption of the molecule investigated. In the present study, EFISH measurements were carried out in $CHCl_3$ solutions, with a non-resonant incident wavelength of 1.907 μm, affording $\mu\beta_{1.907}$ values. To obtain the value of $\beta_{1.907}$, we used the theoretically calculated ground state dipole moment.

All β-ketoimines and BF_2 complexes are characterized by a positive value of $\mu\beta_{1.907}$ (Table 2), in agreement with the positive solvatochromism and the theoretically calculated positive value of $\Delta\mu_{eg}$ (dipole moment difference between the excited and ground state; Table 2) according to the two-level model.[74,75] It turned out that the highest $\mu\beta_{1.907}$ value of β-ketoimines is observed for **L4** which has the strong electron-withdrawing NO_2 group on the phenyl ring (625 x10^{-48} esu, Table 2 and Figure 11), due to the particularly large ground state dipole moment of the molecule (8.574 D). In fact, the $\beta_{1.907}$ value of **L4** (73 x10^{-30} esu) is slightly higher than that of **L3** (50 x10^{-30} esu) with the CN group but much lower than that of **L1** (210 x10^{-30} esu) with no substituent in *para* position of the phenyl group.

Figure 11. Second-order nonlinear optical properties determined by the

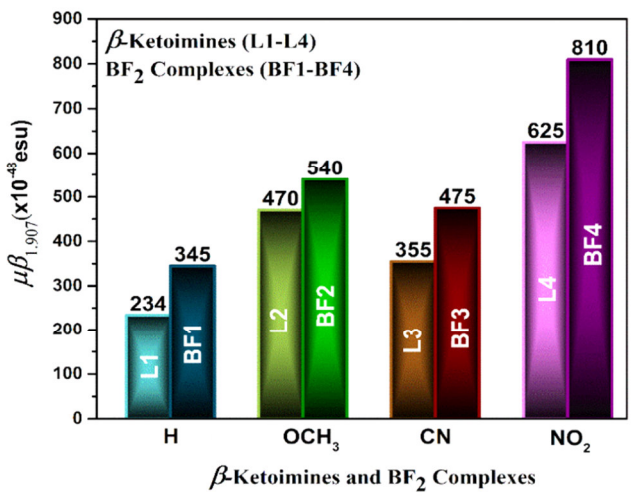

EFISH technique.

The highest value of $\beta_{1.907}$ (460 x10^{-30} esu; Table 2) is observed for **L2** bearing OCH_3, a strong donor group. The $\mu\beta_{1.907}$ values of ketoimines are enhanced upon formation of the corresponding BF_2 complexes, mainly due to an increase of the dipole moments. In the case of **L2**, the large dipole moment enhancement (factor of 6.7) upon formation of **BF2** is counter-balanced by a decrease of the quadratic hyperpolarizability (factor of 5.8), leading to a similar $\mu\beta_{1.907}$ value. The best $\mu\beta_{1.907}$ values are reached with **L4** (625 x 10^{-48} esu) and **BF4** (810 x 10^{-48} esu), bearing the nitro group on the phenyl ring. These compounds are of particular interest from an applicative point of view since their second-order NLO activity is much higher than that of Disperse Red One (*trans*-4,4'-$O_2NC_6H_4N{=}NC_6H_4NEt(CH_2CH_2OH)$] with a $\mu\beta_{1.907}$ of 500 x 10^{-48} esu) which has been used in electrooptic polymeric poled films.[76]

Conclusion

In summary, we designed, synthesized and well characterized a new series of β-ketoimines and related BF_2 complexes. Their absorption spectra showed a positive solvatochromism on increasing the solvent polarity, highlighting the larger polarity of the excited state. Ketoimines exhibited a weak emission due to the presence of excited-state intramolecular proton transfer (ESIPT). However, restriction of the keto-enamine tautomerism, through the formation of -BF_2 complexes, turned out to be an elegant way to increase the luminescence and to improve quantum yields by one order of magnitude. Both β-ketoimines and BF_2 complexes are AIE–active. Substitution of pure CH_3CN by a mixture of CH_3CN/H_2O (1/9 v/v) led to a large increase of their fluorescence quantum yield. The highest enhancement (by a factor of 48) was observed in the case of complex **BF4** bearing the NO_2 group. The AIE effect highlighted in the present work is much larger than that previously observed in the case of ferrocenyl Schiff bases (enhancement of quantum yields by a factor of 4-9 upon addition of a suitable amount of water).[41] The novel β-ketoimines are also NLO-active, their $\mu\beta_{1.907}$ values being enhanced upon formation of the corresponding BF_2 complexes, mainly due to an increase of the dipole moments. Remarkably, the **BF4** complex is characterized by a rather large second-order NLO response, of interest from a practical point of view. These AIE and NLO properties qualify the prepared boron complexes as fascinating multifunctional molecular materials for application in photonics.

Experimental Section

Materials

The 1-(4,4,4-trifluoromethyl-1,3-dione) ferrocene was synthesized following a reported procedure.[46] Column chromatographic separations were carried out using silica gel 60 (AVRA, 100–120 mesh). All other reagents and solvents, purchased from sigma-aldrich and TCI chemicals, were used without prior purification.

Instrumentation

^{1}H NMR and ^{13}C NMR spectra were recorded using a Bruker FT-NMR-400 MHz spectrometer with $CDCl_3$ as solvent and tetramethylsilane as an internal standard. High-resolution mass spectrometry (HRMS) was performed on an Agilent Technologies. FT-IR spectra were obtained using KBr discs with a Shimadzu FT-IR spectrometer (400-4000 cm^{-1}). UV-visible spectra were recorded using a JASCO UV-visible spectrometer using CH_3CN as solvent. Cyclic voltammetry was performed using a CH Instrument model CHI620E. In all electrochemical measurements, 0.1 M Bu_4NClO_4 (TBAP) was used as a supporting electrolyte, and the redox potentials of the complexes were measured against a saturated Ag/AgCl reference electrode. All the $E_{1/2}$ values were calculated from $(E_{pa} + E_{pc})/2$ (pa – anodic potential and pc – cathodic potential) at a scan rate of 50mV s^{-1}. The fluorescence lifetime of both β-ketoimines and BF_2 complexes was measured using a time-correlated single-photon counting (TCSPC) system by means of an Edinburg FLS 980 spectrometer. PL decay dynamics of β-ketoimines and BF_2 complexes AIE-active state emissions were measured with a picosecond xenon Arc lamp of 450 W power. PL decay measurements for lifetimes were carried out with a TCSPC setup from Edinburgh Instruments using a 371 nm Picosecond Pulsed Diode Laser (UK, EPL-375), the analysis being carried out with a F980 software; the goodness of fit was evaluated by fixing χ^2 values between 1.18 and 1.49.

General procedure for the synthesis of β-ketoimines (L1-L4)

1-(4,4,4-trifluoromethyl-1,3-dione) ferrocene (2 mmol) was dissolved in dry toluene (75 ml). The corresponding amine (2 mmol) was added along with a catalytic amount of Al_2O_3 (10 mol%). The reaction mixture was heated and azeotropic removal of water was accomplished using a Dean–Stark apparatus. After 26 h the solution was filtered and evaporation of the solvent gave a red oily substance. The crude product was purified by column chromatography using mixtures of n-hexane:ethyl acetate (9:1 to 8:2) as eluent to obtain the ferrocenyl derivative.

(Z)-4,4,4-trifluoro-1-ferrocenyl-3-(phenylimino)butan-1-one (L1)

According to the general procedure, ketoimine **L1** was isolated as a dark red solid: 636 mg, yield 76%; m.p. 110.2-112.3°C; ^{1}H NMR (400 MHz, $CDCl_3$): δ_H 4.22 (s, 5H, C_5H_5), 4.56 (d, J = 1.2 Hz, 2H, H_β C_5H_4), 4.85 (d, J = 1.2 Hz, 2H, H_α C_5H_4), 5.99 (s, 1H, CH), 7.28 (t, J = 7.8, 6.5 Hz, 3H, C_6H_5), 7.38 (t, J = 7.6 Hz, 2H, C_6H_5), 11.90 (s, 1H, NH); ^{13}C NMR (100 MHz, $CDCl_3$): δ_C 68.97 (C_α C_5H_4), 70.15 (C_5H_5), 72.27 (C_β C_5H_4), 81.05 (C_{ipso} C_5H_4), 94.33 (CH=C), 114.19 (q, $^1J_{C\text{-}F}$ =280 Hz), 117.97 (C–F), 125.53 (C-4), 126.51 (C-3 and C-5), 128.98 (C-2 and C-6), 138.32 (C-1), 145.17 (q, $^2J_{C\text{-}F}$ =30 Hz), 154.62 (N-CH), 196.14 (C=O) ppm; ^{19}F NMR (376 MHz, $CDCl_3$): δ_F –62.2; FT-IR (KBr disk): 3236 (w) ν(N–H), 3091 (w) ν(C–H arom), 2915 (w), ν(C–H aliph), 1666 (s) ν(C=O), 1571 (s) ν(C–O) or ν(C–C), 1448 (m) ν(C–N), 1299 (s) ν(C=C), 1143 (s) ν(C–F), 1082 (m) ν(C=C Fc), 752 (s) ν(C–H arom) cm^{-1}; UV/Vis (CH_3CN): λ_{max}= 276, 326, 484 nm; Fluorescence (CH_3CN): λ_{ex}= 375 nm; λ_{em}= 434 nm; HR-MS (ESI) calcd for m/z: 399.0533; found: 399.0554.

(Z)-4,4,4-trifluoro-3-((4-methoxyphenyl)imino)-1-ferrocenylbutan-1-one (L2)

According to the general procedure, ketoimine **L2** was isolated as a dark red solid: 594 mg, yield 66%; m.p. 88.6-90.3°C; ^{1}H NMR (400 MHz, $CDCl_3$): δ_H 3.74 (s, 3H, OCH_3), 4.15 (s, 5H, C_5H_5), 4.45 (d, J = 1.6 Hz, 2H, H_β C_5H_4), 4.74 (d, J = 1.2 Hz, 2H, H_α C_5H_4), 5.86 (s, 1H, CH), 6.78 (d, J = 8.8 Hz, 2H, C_6H_4), 7.08 (d, J = 8.8 Hz, 2H, C_6H_4), 11.63 (s, 1H, NH); ^{13}C NMR (100 MHz, $CDCl_3$): δ_C 55.43 (OCH_3), 68.92 (C_α C_5H_4), 70.10 (C_5H_5), 72.12 (C_β C_5H_4), 81.10 (C_{ipso} C_5H_4), 93.15 (CH=C), 114.05 (C-3 and C-5), 118.91 (C–F), 121.61 (q, $^1J_{C\text{-}F}$ =270 Hz) 127.59, (C-2 and C-6), 130.91 (C-1), 146.70 (q, $^2J_{C\text{-}F}$ =31 Hz), 149.10 (N-CH), 158.37 (C–O), 195.48 (C=O) ppm; ^{19}F NMR (376 MHz, $CDCl_3$): δ_F –63.2; FT-IR (KBr disk): 3212 (w) ν(N–H), 3137, 3031 (w) ν(C–H arom), 2925 (w), ν(C–H aliph), 1610 (s) ν(C=O), 1504 (s) ν(C–O) or ν(C–C), 1408 (m) ν(C–N), 1254 (s) ν(C=C), 1125 (s) ν(C–F), 1027 (m) ν(C=C Fc), 754 (s) ν(C–H arom) cm^{-1}; UV/Vis (CH_3CN): λ_{max}= 269, 324, 517 nm;

Fluorescence (CH_3CN): λ_{ex}= 375 nm; λ_{em}= 449 nm; HR-MS (ESI) calcd for m/z: 429.0639; found: 429.0662.

Z)-4-((1,1,1-trifluoro-4-oxo-4-ferrocenylbutan-2-ylidene)amino) benzonitrile (L3)

According to the general procedure, ketoimine **L3** was isolated as a dark red solid: 681 mg, yield 77%; m.p. 113.7-115°C; ^{1}H NMR (400 MHz, $CDCl_3$): δ_H 4.15 (s, 5H, C_5H_5), 4.56 (d, *J* = 1.6 Hz, 2H, H_β C_5H_4), 4.68 (d, *J* = 2.1 Hz, 2H, H_α C_5H_4), 6.01 (s, 1H, CH), 7.17 (d, *J* = 6.8 Hz, 2H, C_6H_4), 7.56 (d, *J* = 8.4 Hz, 2H, C_6H_4), 11.97 (s, 1H, NH); ^{13}C NMR (100 MHz, $CDCl_3$): δ_C 69.17 (C_α C_5H_4), 70.31 (C_5H_5), 72.96 (C_β C_5H_4), 81.39 (C_{ipso} C_5H_4), 97.68 (CH=C), 108.63 (C-4), 118.52 (C≡N), 123.56 (q, $^1J_{C\text{-}F}$ =280 Hz), 123.60 (C–F), 123.62, (C-2 and C-6), 133.25 (C-3 and C-5), 142.91 (C-1),143.27 (q, $^2J_{C\text{-}F}$ =36 Hz), 154.18 (N-CH), 196.04 (C=O) ppm; ^{19}F NMR (376 MHz, $CDCl_3$): δ_F –62.4; FT-IR (KBr disk): 3321 (w) ν(N–H), 3085 (w) ν(C–H arom), 2922 (w), ν(C–H aliph), 2221 (w) ν(C≡N), 1628 (s) ν(C=O), 1578 (s) ν(C–O) or ν(C–C), 1470 (m) ν(C–N), 1299 (s) ν(C=C), 1143 (s) ν(C–F), 1001 (m) ν(C=C Fc), 756 (s) ν(C–H arom) cm^{-1}; UV/Vis (CH_3CN): λ_{max}= 271, 327, 514 nm; Fluorescence (CH_3CN): λ_{ex}= 375 nm; λ_{em}= 415nm; HR-MS (ESI) calcd for m/z: 424.0486; found: 424.0506.

(Z)-4,4,4-trifluoro-3-((4-nitrophenyl)imino)-1-ferrocenylbutan-1-one (L4)

According to the general procedure, ketoimine **L4** was isolated as a dark red solid; 801 mg, yield 82%; m.p. 169.2-170.8°C; ^{1}H NMR (400 MHz, $CDCl_3$): δ_H 4.10 (s, 5H, C_5H_5), 4.48 (d, *J* = 1.2 Hz, H_β C_5H_4), 4.71 (d, *J* = 1.2 Hz, H_α C_5H_4), 5.96 (s, 1H, CH), 7.15 (d, *J* = 7.6 Hz, 2H, C_6H_4), 7.51 (d, *J* = 8.8 Hz, 2H, C_6H_4), 11.93 (s, 1H, NH); ^{13}C NMR (100 MHz, $CDCl_3$): δ_C 68.08 (C_α C_5H_4), 69.22 (C_5H_5), 71.88 (C_β C_5H_4), 79.30 (C_{ipso} C_5H_4), 96.60 (CH=C),115.36 (C–F), 117.44 (C-2 and C-6), 122.52 (C-3 and C-5), 122.54 (q, $^1J_{C\text{-}F}$ = 290 Hz), 132.16 (C-4), 141.82 (C-1),141.82 (q, $^2J_{C\text{-}F}$ =31 Hz), 152.23 (N-CH), 194.96 (C=O) ppm; ^{19}F NMR (376 MHz, $CDCl_3$): δ_F –62.4; FT-IR (KBr disk): 3226 (w) ν(N–H), 3097 (w) ν(C–H arom), 2919 (w), ν(C–H aliph), 1668 (s) ν(C=O), 1571 (s) ν(C–O) or ν(C–C), 1533 (s) asym ν(N–O), 1303 (vs) sym ν(N–O), 1413 (m) ν(C–N), 1294 (s) ν(C=C), 1183 (s) ν(C–F), 1006 (m) ν(C=C Fc), 752 (s) ν(C–H arom) cm^{-1}; UV/Vis (CH_3CN): λ_{max}= 268, 322, 515 nm; Fluorescence (CH_3CN): λ_{ex}= 375 nm; λ_{em}= 414 nm; HR-MS (ESI) calcd for m/z: 444.0384; found: 444.0407.

General procedure for the synthesis of boron difluoride complexes (BF1-BF4)

The suitable β-ketoimine **L1-L4** (0.12 mmol) was dissolved in dry dichloromethane (20 mL) and triethylamine (600 mg, 5.92 mmol) was added to the solution. $BF_3{\cdot}OEt_2$ (1020 mg, 7.2 mmol) was then added to the reaction mixture which was at room temperature for 6 h. The solvent was removed with a rotary evaporator, and the crude compound was purified by column chromatography using hexane:ethyl acetate (9:1) as eluent to afford the desired product.

2,2-difluoro-6-ferrocenyl-3-phenyl-4-(trifluoromethyl)-2H-oxazaborinine (BF1)

According to the general procedure, **BF1** was isolated as a purple solid; 859 mg, yield 52%; m.p. 175.4-177.1°C; ^{1}H NMR (400 MHz, $CDCl_3$): δ_H 4.23 (s, 5H, C_5H_5), 4.55 (d, *J* = 1.2 Hz, 2H, H_β C_5H_4), 4.83 (d, *J* = 1.2 Hz, 2H, H_α C_5H_4), 5.98 (s, 1H, CH), 7.28 (t, *J* = 9.4 Hz, 3H, C_6H_5), 7.38 (t, *J* = 7.6 Hz, 2H, C_6H_5); ^{13}C NMR (100 MHz, $CDCl_3$): δ_C 69.30 (C_α C_5H_4), 69.72 (C_5H_5), 69.97 (C_β C_5H_4), 79.29 (C_{ipso} C_5H_4), 92.36 (CH=C), 115.9 (C–F), 118.51 (q, $^1J_{C\text{-}F}$ =280 Hz), 118.57 (C-2 and C-6), 123.18 (C-4), 129.34 (C-3 and C-5), 145.57 (q, $^2J_{C\text{-}F}$ =30 Hz), 146.49 (C-1), 162.43 (C=N), 173.65 (C–O) ppm;^{19}F NMR (376 MHz, $CDCl_3$): δ_F –62.8, –135.6; ^{11}B NMR (128 MHz, $CDCl_3$): δ_B –31.8; FT-IR (KBr disk): 3099 (w) ν(C–H arom), 2921 (w), ν(C–H aliph), 1578 (s) ν(C=N), 1531 (s) ν(C–O) or ν(C–C), 1421 (m) ν(C–N), 1252 (m) ν(C=C), 1177 (s) ν(B–O), 1136 (s) ν(C–F), 1096 (s) ν(B–N), 1028 (m) ν(C=C Fc), 939 (w) ν(B–F), 689 (s) ν(C–H arom) cm^{-1}; UV/Vis (CH_3CN): λ_{max}= 272, 325, 486 nm; Fluorescence (CH_3CN): λ_{ex}= 375 nm; λ_{em}= 449 nm; HR-MS (ESI) calcd for m/z: 447.0516; found: 447.0541.

2,2-difluoro-3-(4-methoxyphenyl)-6-ferrocenyl-4-(trifluoromethyl)-2H-oxazaborinine (BF2)

According to the general procedure, **BF2** was isolated as a purple solid: 920 mg, yield 55%; m.p. 163.2-165.7°C; ^{1}H NMR (400 MHz, $CDCl_3$): δ_H 3.83 (s, 3H, OCH_3), 4.33 (s, 5H, C_5H_5), 4.79 (d, *J* = 1.2 Hz, 2H, H_β C_5H_4), 5.00 (d, *J* = 1.6 Hz, 2H H_α C_5H_4), 6.09 (s, 1H, CH), 6.90 (d, *J* = 6 Hz, 2H, C_6H_4), 7.20 (d, *J* = 6.8 Hz, 2H, C_6H_4); ^{13}C NMR (100 MHz, $CDCl_3$): δ_C 55.43 (OCH_3), 68.92 (C_α C_5H_4), 70.11 (C_5H_5), 72.14 (C_β C_5H_4), 81.09 (C_{ipso} C_5H_4), 93.05 (CH=C), 114.04 (C-3 and C-5), 116.40 (C–F), 121.72 (q, $^1J_{C\text{-}F}$ =270 Hz) 130.89, (C-2 and C-6), 147.28 (C-4),146.13 (q, $^2J_{C\text{-}F}$ =30 Hz), 158.36 (C–O), 164.41 (C=N), 175.11.48 (C–O) ppm; ^{19}F NMR (376 MHz, $CDCl_3$): δ_F –62.3, –137.0; ^{11}B NMR (128 MHz, $CDCl_3$): δ_B –31.7; FT-IR (KBr disk): 3094 (w) ν(C–H arom), 2926 (w), ν(C–H aliph), 1577 (s) ν(C=N), 1521 (s) ν(C–O) or ν(C–C), 1440 (m) ν(C–N), 1299 (m) ν(C=C), 1171 (s) ν(B–O), 1134 (s) ν(C–F), 1103 (s) ν(B–N), 1024 (m) ν(C=C Fc), 934 (w) ν(B–F), 666 (s) ν(C–H arom) cm^{-1}; UV/Vis (CH_3CN): λ_{max}= 267, 328, 514 nm; Fluorescence (CH_3CN): λ_{ex}= 375 nm; λ_{em}= 462 nm; HR-MS (ESI) calcd for m/z: 477.0622; found: 477.0648.

4-(2,2-difluoro-6-ferrocenyl-4-(trifluoromethyl)-2H-oxazaborinin-3-yl)benzonitrile (BF3)

According to the general procedure, **BF3** was isolated as a purple solid: 886 mg, yield 53%; m.p. 116.6-118.3°C; ^{1}H NMR (400 MHz, $CDCl_3$): δ_H 4.08 (s, 5H, C_5H_5), 4.14 (d, *J* = 1.2 Hz, H_β C_5H_4), 4.25 (d, *J* = 1.6 Hz, H_α C_5H_4), 6.75 (s, 1H, CH), 7.45 (d, *J* = 8.8 Hz, 2H, C_6H_4), 8.17 (d, *J* = 9.2 Hz, 2H, C_6H_4); ^{13}C NMR (100 MHz, $CDCl_3$): δ_C 69.53 (C_α C_5H_4), 69.81 (C_5H_5), 70.72 (C_β C_5H_4), 81.70 (C_{ipso} C_5H_4), 93.74 (CH=C), 114.65 (C-4), 117.01 (C≡N), 117.48 (C–F), 118.56 (q, $^1J_{C\text{-}F}$ =280 Hz), 122.33 (C-3 and C-5), 128.21 (C-1), 131.50 (C-2 and C-6), 147.31 (q, $^2J_{C\text{-}F}$ =30 Hz), 158.97 (C=N), 176.19 (C–O) ppm; ^{19}F NMR (376 MHz, $CDCl_3$): δ_F –62.4, –137.2; ^{11}B NMR (128 MHz, $CDCl_3$): δ_B –35.3; FT-IR (KBr disk): 3064 (w) ν(C–H arom), 2930 (w), ν(C–H aliph), 2225 (w) ν(C≡N), 1563 (s) ν(C=N), 1517 (s) ν(C–O) or ν(C–C), 1464 (m) ν(C–N), 1296 (m) ν(C=C), 1190 (s) ν(B–O), 1138 (s) ν(C–F), 1097 (s) ν(B–N), 1028 (m) ν(C=C Fc), 941 (w) ν(B–F), 673 (s) ν(C–H arom) cm^{-1}; UV/Vis (CH_3CN): λ_{max}= 265, 323, 519 nm; Fluorescence (CH_3CN): λ_{ex}= 375 nm; λ_{em}= 435 nm; HR-MS (ESI) calcd for m/z: 472.0469; found: 472.0493.

2,2-difluoro-6-ferrocenyl-3-(4-nitrophenyl)-4-(trifluoromethyl)-2H-oxazaborinine (BF4)

According to the general procedure, **BF4** was isolated as a purple solid: 942 mg, yield 56%; m.p. 187.2-188.7°C; ^{1}H NMR (400 MHz, $CDCl_3$): δ_H 4.15 (s, 5H, C_5H_5), 4.18 (d, *J* = 1.2 Hz, 2H, H_β C_5H_4), 4.28 (d, *J* = 3.2, Hz, 2H, H_α C_5H_4), 6.79 (s, 1H, CH), 7.52 (d, *J* = 8.0 Hz, 2H, C_6H_4), 7.67 (d, *J* = 8.0 Hz, 2H, C_6H_4); ^{13}C NMR (100 MHz, $CDCl_3$): δ_C 69.07 (C_α C_5H_4), 69.29 (C_5H_5), 69.66 (C_β C_5H_4), 81.25 (C_{ipso} C_5H_4), 93.15 (CH=C), 122.72 (q, $^1J_{C\text{-}F}$ =290 Hz), 123.45 (C–F), 127.59 (C-3 and C-5), 132.19 (C-2 and C-6), 138.45 (C-1), 143.86 (q, $^2J_{C\text{-}F}$ =31 Hz), 149.93 (C-4), 162.35 (C=N), 176.23 (C–O) ppm; ^{19}F NMR (376 MHz, $CDCl_3$): δ_F –63.2, –136.7; ^{11}B NMR (128 MHz, $CDCl_3$): δ_B –35.6; FT-IR (KBr disk): 3091 (w) ν(C–H arom), 2930 (w), ν(C–H aliph), 1574 (s) ν(C=N), 1517 (s) asym ν(N–O), 1306 (vs) sym ν(N–O), 1456 (m) ν(C–N), 1297 (m) ν(C=C), 1187 (s) ν(B–O), 1142 (s) ν(C–F), 1098 (s) ν(B–N), 1014 (m) ν(C=C Fc), 942 (w) ν(B–F), 671 (s) ν(C–H arom) cm^{-1};UV/Vis (CH_3CN): λ_{max}= 257, 314, 533 nm; Fluorescence (CH_3CN): λ_{ex}= 375 nm; λ_{em}= 438 nm; HR-MS (US) calcd for m/z: 492.0367; found: 492.0392.

Single-crystal X-ray structure determination of chromophores L1, L2, L3 and BF1

All crystals were obtained by slow evaporation of the corresponding solutions (ethyl acetate/hexane) at room temperature. Crystals were stored in paraffin-oil, mounted in a MiTeGen loop, and measured at 296 K. The crystal approximate dimensions are 0.60 x 0.30 x 0.20 mm^3 (for **L1**), 0.30 x 0.20 x 0.20 mm^3 (for **L2** and **L3**), and 0.35 x 0.35 x 0.30 mm^3 (for **BF1**). The X-ray diffraction data was collected on an Agilent SuperNova (Oxford Diffraction) diffractometer using Mo-K_α radiation (λ = 0.71073 Å). The Apex2 package was used for cell refinements and data reductions. The structures were solved by direct methods using the Shelxs 97 or Superflip program[77] with the Olex 2 graphical user interface.[78] Structural refinements were carried out using Shelxl-97 or Shelxl-2014. The positions of all the atoms were obtained by direct methods and the crystallographic details were summarized in (Table S1).

Procedure of ESIPT studies for ketoimine (L1)

A stock solution of ketoimine **L1** and boron trifluoride diethyl etherate ($BF_3{\cdot}OEt_2$) were freshly prepared in CH_3CN before testing each performance. To perform this experiment, we have prepared 10 mL of a $2{\times}10^{-5}$ M solution of ketoimine **L1** by adding 40μL of a $1{\times}10^{-3}$ M solution by the serial dilution method, and the $1{\times}10^{-3}$ M stock solution was prepared by dissolving 4.21 mg of ketoimine **L1** in 10 mL of CH_3CN. Then, 143 μL of $BF_3{\cdot}OEt_2$ was dissolved in 10 mL of CH_3CN, which gave $1{\times}10^{-1}$ M concentration. Furthermore, increasing concentrations of $BF_3{\cdot}OEt_2$ (0-270 μM) solution were directly used for **L1**, for the absorption and fluorescence experiments. The solution of $BF_3{\cdot}OEt_2$ ($1{\times}10^{-1}$ M) was added dropwise to the solution of ketoimine **L1** (2 mL of 20μM) by gently mixing until the disappearance of orange-red color, observed by the naked eye, suggesting the formation of the boron difluoride complex (**BF1**). The emission color changed from weak orange-red to strong violet blue at 413 nm. The fluorescence maxima of ketoimine **L1** at 413 nm was observed with excitation emission wavelength at 375 nm.

Determination of the quantum yields

The fluorescence quantum yields (Φ) were determined by equation (4) concerning Quinine Sulphate (Φ_{st} = 0.50 in H_2SO_4).[79]

$$\Phi_x = \Phi_{st} \times \left[\frac{A_{st}}{A_x}\right] \times \left[\frac{I_x}{I_{st}}\right] \times \left[\frac{\eta_x^2}{\eta_{st}^2}\right] \quad (4)$$

Subscripts "*x*" and "*st*" stand for unknown and standard (quinine sulphate) sample respectively; "*Φ*" for quantum yield, "*A*" for absorbance, "*η*" for the refractive index of the solvents, "*I*" is the area under the fluorescence spectra on an energy scale. The fluorescence lifetime measurement was carried out using a single photon counting method. The fluorescence decay curve was measured by exciting the molecule at 290 nm, in <200 ps light using nano LED.

Computational details

The density functional theory (DFT) based calculations were performed using the Gaussian 16 Revision C.01 program.[80] The selection of functional and combination of the basis set is based on the theory, defined bonding patterns, electronic charge, and molecular orbital energy distributions. The time-dependent DFT (TD-DFT) method was used to investigate the origin of electronic absorption spectra. The geometries of β-ketoimines and complexes in the solvent phase were optimized using Becke's three-parameter[81] and Lee–Yang–Parr functional (B3LYP); the B3LYP functional was combined with the 6-31+G** basis set for all the calculations.[82] The two states, in the case of simple dipolar *push-pull* systems exhibiting a single dominant absorption band, are generally the ground and the first excited state (the so-called two-level model).[74-75] The electronic geometries and frontier molecular orbital structures were defined using the Gauss View 6.1.1 molecular visualization program.[83]

EFISH measurements

The second-order nonlinear optical properties were determined by means of the electric field induced second harmonic generation (EFISH) technique in solution.[71-73] The EFISH cell consisted of a stainless steel container with two quartz optical windows that form a wedge-shaped cavity within the cell and the electrode was connected to the high voltage supply. The cell was mounted on an electrically isolated translation stage. The whole-cell was then translated horizontally relative to the incident beam to produce fringes at the second harmonic wavelength. Every measurement was referenced separately to the fringes of the pure solvent ($CHCl_3$), that was used to dissolve the chromophore, to consider laser power's fluctuations.

Acknowledgements

We gratefully acknowledge the DST Indo-Italian Joint Project (no. INT/Italy/P-15/2016(SP) and the "Ministero degli Affari Esteri e della Cooperazione Internazionale" (bilateral project Italy India, Prot. no. MAE0065640) for financial support. We are very grateful to VIT-SIF, for providing instrumental facilities, and to STIC-India, Cochin for providing the single-crystal XRD data. We are very much thankful to Inorganic and Physical Chemistry Lab, CSIR-CLRI, Chennai for Lifetime studies. Also, we deeply thank Stefania Righetto for EFISH measurements and Dominique Roberto for fruitful discussions.

Keywords: nonlinear optics • excited-state intramolecular proton transfer (ESIPT) • aggregation-induced emission (AIE) • DFT calculations • electric field induced second harmonic generation (EFISH)

[1] P. N. Prasad, D. J. Williams, *Introduction to nonlinear optical effects in molecules and polymers*, Wiley New York, 1991, vol. 1.
[2] J. Zyss, *Molecular nonlinear optics: materials, physics and devices*, Academic Press, Boston, 2013.
[3] H. S. Nalwa, *Appl. Organomet. Chem.* **1991**, 5, 349–377.
[4] S. S. M. Fernandes, C. Herbivo, J. Aires-de-Sousa, A. Comel, M. Belsley, M. M. M. Raposo, *Dyes Pigm.* **2018**, 149, 566–573.
[5] S. Di Bella, I. P. Oliveri, A. Colombo, C. Dragonetti, S. Righetto, D. Roberto, *Dalton Trans.* **2012**, 41, 7013–7016.
[6] E. Cariati, C. Dragonetti, E. Lucenti, F. Nisic, S. Righetto, D. Roberto, E. Tordin, *Chem. Commun.* **2014**, 50, 1608–1610.
[7] B. J. Coe, *Acc. Chem. Res.* **2006**, 39, 383–393.
[8] J. Heck, M. Dede, *Ferrocene-Based Electro-Optical Materials, In Ferrocenes: Ligands, Materials and Biomolecules*, (Eds.: P. Stepnika), John Wiley & Sons, Ltd, **2008**, Chapter 9, pp. 319-392.
[9] S. J. Mathews, S. C. Kumar, L. Giribabu, S. V. Rao, *Mater. Lett.* **2007**, 61, 4426–4431.
[10] D. R. Kanis, P. G. Lacroix, M. A. Ratner, T. J. Marks, J. Am. Chem. Soc. **1994**, 116, 10089–10102.
[11] a) N. Novoa, T. Roisnel, P. Hamon, S. Kahlal, C. Manzur, H. M. Ngo, I. Ledoux-Rak, J.-Y. Saillard, D. Carrillo, J.-R. Hamon, *Dalton Trans.* **2015**, 44, 18019–18037; b) V. Artigas, D. González, M. Fuentealba, *J. Mol. Struct.* **2017**, 1129, 325–332; c) S. Celedon, M. Fuentealba, T. Roisnel, J.-R. Hamon, D. Carrillo, C. Manzur, *Inorg. Chim. Acta* **2012**, 390, 184–189; d) M. Fuentealba, A. Trujillo, J.-R. Hamon, D. Carrillo, C. Manzur, *J. Mol. Struct.* **2008**, 881, 76–82.
[12] C. Karthika, S. R. Sarath Kumar, L. Kathuria, P. K. Das, A. G. Samuelson, *Phys. Chem. Chem. Phys.* **2019**, 21, 11079–11086.

[13] F. Tessore, D. Roberto, R. Ugo, P. Mussini, S. Quici, I. Ledoux‐Rak, J. Zyss, *Angew. Chem. Int. Ed.* **2003**, 42, 456‐459.

[14] M. Pizzotti, R. Ugo, C. Dragonetti, E. Annoni, F. Demartin, P. Mussini, *Organometallics* **2003**, 22, 4001–4011.

[15] J. P. Morrall, G. T. Dalton, M. G. Humphrey, M. Samoc, *Adv. Organomet. Chem.* **2007**, 55, 61–136.

[16] S. Di Bella, C. Dragonetti, M. Pizzotti, D. Roberto, F. Tessore and R. Ugo in Coordination and Organometallic Complexes as Second-Order Nonlinear Optical Molecular Materials, Vol. 28 (Eds.: H. Bozec and V. Guerchais), Springer Berlin Heidelberg, Berlin, Heidelberg, **2010**, pp. 1-55.

[17] A. Colombo, C. Dragonetti, V. Guerchais, C. Hierlinger, E. Zysman-Colman, D. Roberto, *Coord. Chem. Rev.* **2020**, 414, 213293.

[18] a) M. Watanabe, Y. Jay, P. Chou, A. Staykov, M. Shibahara, K. Sako, T. Ishihara, T. J. Chow, *Tetrahedron Lett.* **2015**, 56, 1548–1551; b) D. Astruc, *Eur. J. Inorg. Chem.* **2017**, 2017, 6–29.

[19] A. Ion, M. Buda, J. C. Moutet, E. Saint-Aman, G. Royal, I. Gautier-Luneau, M. Bonin, R. Ziessel, *Eur. J. Inorg. Chem.* **2002**, 2, 1357–1366.

[20] M. Saleem, H. Yu, L. Wang, Zain-ul-Abdin, H. Khalid, M. Akram, N. M. Abbasi, J. Huang, *Anal. Chim. Acta* **2015**, 876, 9–25.

[21] M. L. H. Green, S. R. Marder, M. E. Thompson, J. a Bandy, D. Bloor, P. V Kolinsky, R. J. Jones, *Nature*. **1987**, 330, 360–362.

[22] V. Alain, M. Blanchard-Desce, C. T. Chen, S. R. Marder, A. Fort, M. Barzoukas, *Synth. Met.* **1996**, 81, 133–136.

[23] a) S. Barlow, S. R. Marder, *Chem. Commun.* **2000**, 1555–1562; b) S. Kaur, M. Kaur, P. Kaur, K. Clays, K. Singh, *Coord. Chem. Rev.* **2017**, 343, 185–219.

[24] S. Salman, J.-L. Brédas, S. R. Marder, V. Coropceanu, S. Barlow, *Organometallics* **2013**, 32, 6061–6068.

[25] M. Zaarour, A. Singh, C. Latouche, J. A. G. Williams, I. Ledoux-Rak, J. Zyss, A. Boucekkine, H. Le Bozec, V. Guerchais, C. Dragonetti, *Inorg. Chem.* **2013**, 52, 7987–7994.

[26] N. Palanisami, I. S. Moon, *Sci. Adv. Mater.* **2014**, 6, 2378–2383.

[27] K. Senthilkumar, M. Pizzotti, K. Thirumoorthy, G. Di Carlo, S. Righetto, A. Orbelli Biroli, M. Haukka, N. Palanisami, *J. Phys. Chem. C* **2016**, 120, 20277–20287.

[28] K. Senthilkumar, K. Thirumoorthy, C. Dragonetti, D. Marinotto, S. Righetto, A. Colombo, M. Haukka, N. Palanisami, *Dalton Trans.* **2016**, 45, 11939–11943.

[29] S. Prabu, E. David, T. Viswanathan, K. Thirumoorthy, T. Panda, C. Dragonetti, A. Colombo, D. Marinotto, S. Righetto, D. Roberto, N. Palanisami, *Dalton Trans*. **2020**, 49, 1854–1863.

[30] R. Teimuri-Mofrad, K. Rahimpour, R. Ghadari, S. Ahmadi-Kandjani, *J. Mol. Liq.* **2017**, 244, 322–329.

[31] a) A. Matei, C. Constantinescu, V. Ion, B. Mitu, I. Ionita, M. Dinescu, C. Vasiliu, A. Emandi, *J. Organomet. Chem.* **2014**, 751, 638–643; b) A. Trujillo, M. Fuentealba, D. Carrillo, C. Manzur, I. Ledoux-Rak, J. R. Hamon, J. Y. Saillard, *Inorg. Chem.* **2010**, 49, 2750–2764; c) N. Novoa, C. Manzur, T. Roisnel, V. Dorcet, N. Cabon, F. Robin-Le Guen, I. Ledoux-Rak, S. Kahlal, J. Y. Saillard, D. Carrillo, J. R. Hamon, *New J. Chem.* **2019**, 43, 10468–10481; d) S. Celedón, T. Roisnel, V. Artigas, M. Fuentealba, D. Carrillo, I. Ledoux-Rak, J.-R. Hamon, C. Manzur, *New J. Chem.* **2020**, 44, 9190–9201.

[32] E. Cariati, D. Roberto, R. Ugo, P. C. Ford, S. Galli, A. Sironi, *Chem. Mater.* **2002**, 14, 5116–5123.

[33] J. Boixel, V. Guerchais, H. Le Bozec, A. Chantzis, D. Jacquemin, A. Colombo, C. Dragonetti, D. Marinotto, D. Roberto, *Chem. Commun.* **2015**, 51, 7805–7808.

[34] A. Colombo, C. Dragonetti, D. Marinotto, S. Righetto, D. Roberto, S. Tavazzi, M. Escadeillas, V. Guerchais, H. Le Bozec, A. Boucekkine, *Organometallics* **2013**, 32, 3890–3894.

[35] V. Guerchais, L. Ordronneau, H. Le Bozec, *Coord. Chem. Rev*. **2010**, 254, 2533–2545.

[36] H. Zhao, E. Garoni, T. Roisnel, A. Colombo, C. Dragonetti, D. Marinotto, S. Righetto, D. Roberto, D. Jacquemin, J. Boixel, V. Guerchais, *Inorg. Chem.* **2018**, 57, 7051–7063.

[37] P. Matozzo, A. Colombo, C. Dragonetti, S. Righetto, D. Roberto, P. Biagini, S. Fantacci, D. Marinotto, *Inorganics* **2020**, 8, 25.

[38] J. Luo, Z. Xie, J. W. Y. Lam, L. Cheng, B. Z. Tang, H. Chen, C. Qiu, H. S. Kwok, X. Zhan, Y. Liu, D. Zhu, *Chem. Commun*. **2001**, 1740–1741.

[39] Y. Hong, J. W. Y. Lam, B. Z. Tang, *Chem. Soc. Rev*. **2011**, 40, 5361–5388.

[40] S. K. Lanke, N. Sekar, *Dyes Pigm*. **2016**, 124, 82–92.

[41] E. David, K. Thirumoorthy, N. Palanisami, *Appl. Organomet. Chem.* **2018**, 32, e4522.

[42] A. C. Sedgwick, L. Wu, H. H. Han, S. D. Bull, X. P. He, T. D. James, J. L. Sessler, B. Z. Tang, H. Tian, J. Yoon, *Chem. Soc. Rev.* **2018**, 47, 8842–8880.

[43] X. Bi, B. Liu, L. McDonald, Y. Pang, *J. Phys. Chem. B* **2017**, 121, 4981–4986.

[44] V. S. Padalkar, Y. Tsutsui, T. Sakurai, D. Sakamaki, N. Tohnai, K. Kato, M. Takata, T. Akutagawa, K. I. Sakai, S. Seki, *J. Phys. Chem. B* **2017**, 121, 10407–10416.

[45] K. Tanaka, Y. Chujo, *NPG Asia Mater.* **2015**, 7, e223–e223.

[46] Q. Zhang, W. L. Song, A. M. Showkot Hossain, Z. Di Liu, G. J. Hu, Y. P. Tian, J. Y. Wu, B. K. Jin, H. P. Zhou, J. X. Yang, S. Y. Zhang, *Dalton Trans.* **2011**, 40, 3510–3516.

[47] Y. Suwa, M. Yamaji, *J. Photochem. Photobiol. A* **2016**, 329, 146–148.

[48] Y. C. Shi, C. X. Sui, H. Bin Song, P. M. Jian, *J. Coord. Chem.* **2005**, 58, 363–371.

[49] M. M. Conradie, A. J. Muller, J. Conradie, *South African J. Chem.* **2008**, 61, 13–21.

[50] U. Balijapalli, S. K. Iyer, European *J. Org. Chem.* **2015**, 2015, 5089–5098.

[51] S. Rani, P. Mourya, M. M. Singh, V. P. Singh, *J. Organomet. Chem.* **2014**, 767, 136–143.

[52] S. Prabu, E. David, T. Viswanathan, J. S. Angelin Jinisha, R. Malik, K. Rudharachari Maiyelvaganan, M. Prakash, N. Palanisami, *J. Mol. Struct.* **2020**, 1202, 127302.

[53] J. Kulhánek, F. Bureš, W. Kuznik, I. V. Kityk, T. Mikysek, A. Růžička, *Chem.: Asian J.* **2013**, 8, 465–475.

[54] N. Palanisami, K. Senthilkumar, K. Thirumoorthy, I. S. Moon, *Sci. Adv. Mater.* **2014**, 6, 2364–2369.

[55] U. Warde, N. Sekar, *Dyes Pigm.* **2017**, 137, 384–394.

[56] R. Balasaravanan, V. Sadhasivam, G. Sivaraman, A. Siva, *Asian J. Org. Chem.* **2016**, 5, 399–410.

[57] Y. Wang, G. Lai, Z. Li, Y. Ma, Y. Shen, C. Wang, *Tetrahedron* **2015**, 71, 2761–2767.

[58] Š. Budzák, D. Jacquemin, *Phys. Chem. Chem. Phys.* **2018**, 20, 25031–25038.

[59] S. Kothavale, Y. Erande, N. Sekar, *ChemistrySelect* **2017**, 2, 5013–5024.

[60] S. Sahu, M. Das, A. K. Bharti, G. Krishnamoorthy, *Phys. Chem. Chem. Phys.* **2018**, 20, 27131–27139.

[61] V. Kachwal, P. Alam, H. R. Yadav, S. S. Pasha, A. Roy Choudhury, I. R. Laskar, *New J. Chem.* **2018**, 42, 1133–1140.

[62] Y. Q. Cao, Y. Xi, X. Y. Teng, Y. Li, X. Yan, L. Chen, *Dyes Pigm.* **2017**, 137, 75–83.

[63] E. David, T. Viswanathan, S. Prabu, N. Palanisami, *New J. Chem.* **2019**, 43, 8539–8550.

[64] J. Jayabharathi, K. Jayamoorthy, V. Thanikachalam, *Spectrochim. Acta Part A* **2013**, 101, 156–161.

[65] P. Wang, Y. Tang, X. Wen, R. Amal, Y. H. Ng, *ACS Appl. Mater. Interfaces* **2015**, 7, 19887–19893.

[66] R. Bakthavatsalam, A. Biswas, M. Chakali, P. R. Bangal, B. P. Kore, J. Kundu, *J. Phys. Chem. C* **2019**, 123, 4739–4748.

[67] R. J. Vázquez, H. Kim, B. M. Kobilka, B. J. Hale, M. Jeffries-El, P. Zimmerman, T. Goodson, *J. Phys. Chem. C* **2017**, 121, 14382–14392.

[68] C. Yu, L. Jiao, P. Zhang, Z. Feng, C. Cheng, Y. Wei, X. Mu , E. Hao, *Org. Lett.* **2014**, 16, 3048–3051.

[69] J. Pei, S. Peng, J. Shi, Y. Liang, Z. Tao, J. Liang, *J. Chen, J. Power Sources.* **2009**, 187, 620–626.

[70] B. Possato, V. M. Deflon, Z. Naal, A. L. B. Formiga, S. Nikolaou, *Dalton Trans.* **2017**, 46, 7926–7938.

[71] I. Ledoux, J. Zyss, *Chem. Phys.* **1982**, 73, 203–213.

[72] B. F. Levine, C. G. Bethea, *Appl. Phys. Lett.* **1974**, 24, 445–447.

[73] B. F. Levine, C. G. Bethea, *J. Chem. Phys.* **1975**, 63, 2666–2682.

[74] J.-L. Oudar, D. S. Chemla, *J. Chem. Phys.* **1977**, 66, 2664–2668.

[75] J. L. Oudar, *J. Chem. Phys.* **1977**, 67, 446–457.
[76] K. D. Singer, J. E. Sohn, L. A. King, H. M. Gordon, H. E. Katz, C. W. Dirk, *JOSA B* **1989**, 6, 1339-1350.
[77] G. M. Sheldrick, *Acta Crystallogr. Sect. A: Found. Crystallogr.* **2008**, 64, 112–122.
[78] O. V. Dolomanov, L. J. Bourhis, R. J. Gildea, J. A. K. Howard, H. Puschmann, *J. Appl. Crystallogr.* **2009**, 42, 339–341.
[79] W. H. Melhuish, *J. Phys. Chem.* **1961**, 65, 229–235.
[80] M. J. Frisch, G. W. Trucks, H. B. Schlegel, G. E. Scuseria, M. A. Robb, J. R. Cheeseman, G. Scalmani, V. Barone, G. A. Petersson, H. Nakatsuji, X. Li, M. Caricato, A. V Marenich, J. Bloino, B. G. Janesko, R. Gomperts, B. Mennucci, H. P. Hratchian, J. V Ortiz, A. F. Izmaylov, J. L. Sonnenberg, D. Williams-Young, F. Ding, F. Lipparini, F. Egidi, J. Goings, B. Peng, A. Petrone, T. Henderson, D. Ranasinghe, V. G. Zakrzewski, J. Gao, N. Rega, G. Zheng, W. Liang, M. Hada, M. Ehara, K. Toyota, R. Fukuda, J. Hasegawa, M. Ishida, T. Nakajima, Y. Honda, O. Kitao, H. Nakai, T. Vreven, K. Throssell, J. A. J. Montgomery, J. E. Peralta, F. Ogliaro, M. J. Bearpark, J. J. Heyd, E. N. Brothers, K. N. Kudin, V. N. Staroverov, T. A. Keith, R. Kobayashi, J. Normand, K. Raghavachari, A. P. Rendell, J. C. Burant, S. S. Iyengar, J. Tomasi, M. Cossi, J. M. Millam, M. Klene, C. Adamo, R. Cammi, J. W. Ochterski, R. L. Martin, K. Morokuma, O. Farkas, J. B. Foresman, D. J. Fox, *Gaussian 16, Revis. C.01*, Gaussian, Inc., Wallington, CT, **2016**.
[81] A. D. Becke, *J. Chem. Phys.* 1993, 98, 5648–5652.
[82] C. Lee, W. Yang, R. G. Parr, *Phys. Rev. B* 1**988**, 37, 785–789.
[83] R. Dennington, T. A. Keith, J. M. Millam, *GaussView, Version 6.1*, Semichem Inc., Shawnee Mission. KS, **2016**.

Entry for the Table of Contents

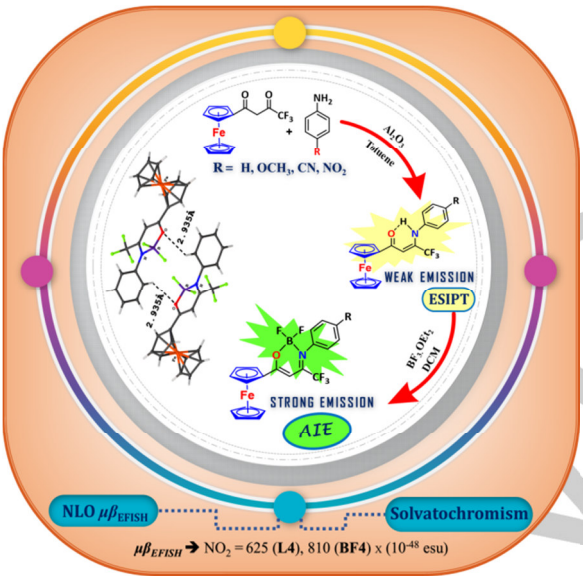

Novel ferrocene-appended β-ketoimines and their BF_2 derivatives for both aggregation-induced emission and large second-order nonlinear optical properties.